

# Optimizing Random Mixup with Gaussian Differential Privacy

Donghao Li <sup>\*</sup>      Yang Cao <sup>†</sup>      Yuan Yao <sup>‡</sup>

February 15, 2022

## Abstract

Differentially private data release receives rising attention in machine learning community. Recently, an algorithm called DPMix is proposed to release high-dimensional data after a random mixup of degree  $m$  with differential privacy. However, limited theoretical justifications are given about the “sweet spot  $m$ ” phenomenon, and directly applying DPMix to image data suffers from severe loss of utility. In this paper, we revisit random mixup with recent progress on differential privacy. In theory, equipped with Gaussian Differential Privacy with Poisson subsampling, a tight closed form analysis is presented that enables a quantitative characterization of optimal mixup  $m^*$  based on linear regression models. In practice, mixup of features, extracted by handcraft or pre-trained neural networks such as self-supervised learning without labels, is adopted to significantly boost the performance with privacy protection. We name it as Differentially Private Feature Mixup (DPFMix). Experiments on MNIST, CIFAR10/100 are conducted to demonstrate its remarkable utility improvement and protection against attacks.

arXiv:2202.06467v1 [cs.LG] 14 Feb 2022

---

<sup>\*</sup>Department of Mathematics, Hong Kong University of Science and Technology. Email: donghao.li@connect.ust.hk

<sup>†</sup>Department of Mathematics, Hong Kong University of Science and Technology. Email: ycaoau@connect.ust.hk

<sup>‡</sup>Department of Mathematics, Hong Kong University of Science and Technology. Email: yuany@ust.hk

# Contents

<b>1</b>	<b>Introduction</b>	<b>3</b>
<b>2</b>	<b>Random Feature Mixup with Gaussian Differential Privacy</b>	<b>4</b>
<b>3</b>	<b>Optimizing the Mixup Degree</b>	<b>6</b>
3.1	Main Results . . . . .	6
3.2	Simulation and Discussion . . . . .	7
3.3	Comparison with Theorem 2 in Lee et al. (2019) . . . . .	7
<b>4</b>	<b>Experiments</b>	<b>8</b>
4.1	Experiment Setup . . . . .	8
4.2	Improvements from GDP with Poisson Sampling . . . . .	8
4.3	Improving Utility via Feature Mixup . . . . .	8
4.4	Hyper-parameter Tuning of DPFMix . . . . .	9
4.5	Utility Comparisons with Other methods . . . . .	10
<b>5</b>	<b>Attacking DPFMix</b>	<b>10</b>
5.1	Model Inversion Attack . . . . .	10
5.2	Membership Inference . . . . .	10
<b>6</b>	<b>Conclusion</b>	<b>11</b>
<b>A</b>	<b>Related Works</b>	<b>15</b>
A.1	Differential Privacy . . . . .	15
A.2	Differentially Private Data Release Algorithms . . . . .	15
A.3	DPSGD . . . . .	16
A.4	Mixup and Its Extension to PPML . . . . .	16
A.5	Attacking Algorithms . . . . .	16
<b>B</b>	<b><math>f</math>-DP framework</b>	<b>17</b>
B.1	$f$ -Differential Privacy . . . . .	17
B.2	Subsampling with $f$ -Differential Privacy . . . . .	18
B.3	Composition with $f$ -Differential Privacy . . . . .	18
B.4	CLT approximation with $\mu$ -GDP . . . . .	18
B.5	Connection between $\mu$ -GDP and $(\epsilon, \delta)$ -DP . . . . .	18
<b>C</b>	<b>Privacy analysis for DPFMix</b>	<b>19</b>
C.1	Proof for Theorem 2.1 . . . . .	19
C.1.1	Single-step of Algorithm 1 . . . . .	19
C.1.2	Composition . . . . .	19
C.1.3	CLT approximation . . . . .	19
C.1.4	Actual noise . . . . .	20
C.2	DP Guarantee with Renyi-DP . . . . .	21
<b>D</b>	<b>Training with noisy mixup labels</b>	<b>21</b>
<b>E</b>	<b>Implementation Detail of Experiments</b>	<b>21</b>
E.1	Datasets . . . . .	21
E.2	Network Structure . . . . .	22
E.3	Detailed Settings for DPFMix and Baselines . . . . .	22
<b>F</b>	<b>Omitted experiment results</b>	<b>23</b>
<b>G</b>	<b>Model Inversion Attack</b>	<b>23</b>
<b>H</b>	<b>Proof of Theorem 3.1</b>	<b>25</b>

# 1 Introduction

Privacy protection in data collection receives a rising attention in human society with new privacy laws, for example, EU General Data Protection Regulation (GDPR). The area of privacy-preserving machine learning (PPML) thus becomes increasingly influential.

Federated learning [McMahan et al. \(2017\)](#) is perhaps the most popular PPML framework. By exchanging gradients of private data, federated learning allows training neural networks without sharing the raw data. However, attackers can reconstruct input data from released gradients [Zhu & Han \(2020\)](#), which makes federated learning not safe to protect data. Split learning [Vepakomma et al. \(2018\)](#) splits the network into two parts and features are sent from the data owner to the central server. Split learning assumes that transforming data into features can avoid privacy leakage. However, attackers can still recover the data based on the released features [He et al. \(2019\)](#).

Both federated learning and split learning can be regarded as algorithms that release transformed information of the private dataset. However, such transformations without rigorous privacy guarantees can be reversible and fail to protect privacy. Differential privacy (DP) [Dwork et al. \(2014\)](#) is a notion of privacy widely adopted in both academic research and industrial applications ([Kenthapadi et al., 2019](#)), for example, Google’s RAPPOR [Erlingsson et al. \(2014\)](#), LinkedIn’s PriPeARL [Kenthapadi & Tran \(2018\)](#), local differential private data collecting system of Apple [Apple \(2017\)](#) and Microsoft [Ding et al. \(2017\)](#). By constraining the worst-case difference between functions of two adjacency datasets that only differ one element, DP makes it hard to tell whether a sample is in or not in the dataset.

A natural way to conduct differentially private learning is that the data owner releases a DP version of data or the transformed one so that others could build machine learning models upon them. Many researchers ([Zhang et al., 2017b](#); [Xu et al., 2017](#); [Lee et al., 2019](#); [Xie et al., 2018](#); [Zhang et al., 2018](#); [Acs et al., 2018](#)) have noticed this direction and proposed some algorithms. One typical algorithm is PrivBayes ([Zhang et al., 2017b](#)). PrivBayes build a noise-injected Bayes network for the private data to model the joint distribution of the data. Then PrivBayes releases synthetic data sampled from the Bayes network. However, these methods face the curse of dimension and can not release high-dimensional data effectively and efficiently. DPPro ([Xu et al., 2017](#)) tried to use random projection to reduce the dimension of the features so that avoid the curse of dimension. However, the random projection will damage the performance and the curse of dimension still exists. Previous works only focus on tabular data with feature dimensions less than 100. Yet, [Lee et al. \(2019\)](#) showed that they fail to handle high dimensional image data which consists of hundreds and thousands of dimensions.

Inspired by the mixup of data for training ([Zhang et al., 2017a](#)), a DP data publishing algorithm called DPMix ([Lee et al., 2019](#)) achieves DP by averaging input data and label with additive DP noise. By mixing the several samples, DPMix reduces the sensitivity of the released data. The key observation of DPMix is that there exists a “sweet spot” on the number of mixup samples (mixup degree)  $m$  that maximizes the utility for a given privacy budget. However, [Lee et al. \(2019\)](#) just give some intuitive analysis without rigorous justification. Moreover, just choosing a suitable  $m$  is not enough to achieve reasonable utility and DPMix suffers from a low utility, for example, a CNN trained on the DPMix CIFAR10 dataset with  $(30, 10^{-5})$ -DP only achieves 26.90% accuracy in ([Lee et al., 2019](#)).

In this paper, we revisit DPMix and found there are two factors that prevent DPMix from a reasonable utility. First, DPMix employs Renyi-DP with uniform subsampling ([Wang et al., 2019](#)) as its DP accountant. However, comparing with recently proposed Gaussian Differential Privacy (GDP) ([Dong et al., 2021](#); [Bu et al., 2020](#)), Renyi-DP with uniform subsampling scheme gives loose and complicated privacy analyses for DPMix. Second, mixup at pixel-level causes a large utility loss. As reported in ([Lee et al., 2019](#)), pixel-level mixup alone without DP noise causes large utility decay. The utility can be even worse if we add DP noise, which would cause overfitting.

To address the two problems, we explore DPMix with GDP and feature mixup in this paper.

In theory, we investigate the effect of  $m$  on the error of the least square estimator in linear regression models. Thanks to the analytically tractable expressions offered by GDP, we derive via random matrix theory an asymptotic upper bound for the error of the least square estimator and show that there exists an optimal  $m^* = O\left(n^{\frac{2-\gamma}{2}}\right)$  that can minimize the error caused by both random mixup and DP noise when the mixup sample size  $T = O(n^\gamma)$  for  $1 \leq \gamma < 2$ . Such an optimal order of  $m^*$  meets the simulation experiments. It particularly improves a partial observation in [Lee et al. \(2019\)](#) that the error of DPMix for linear regression models is monotonically decreasing w.r.t.  $m$  when  $m \ll n$ , which is incomplete without considering the random matrix effect of extreme eigenvalues.

In practice, we find that when handcrafted features or pre-trained neural networks, particularly self-supervised model features, are used as feature extractors before mixup, the utility can be boosted by a large margin. We name it DPFMix since the mixup happens at the feature level. Feature extractors help DPFMix in two ways. First, compared with the pixel-level mixup, the feature mixup allows DPFMix to increase mixed samples without severe utility decay. Second, using a combination of powerful feature extractors and linear classifiers could take advantage of larger models and avoid overfitting at the same time. Empirical evidence are shown on several computer vision datasets. For example, DPFMix with  $(8, 10^{-5})$ -DP can achieve 94.32%, 90.83%, and 66.35% test accuracy on MNIST, CIFAR10, and CIFAR100 datasets, using feature extractors by ScatteringNet and self-supervised ResNet-152 pretrained by SimCLRv2, respectively. Apart from tight DP guarantees, we also show DPFMix could successfully defend two attacks,

---

**Algorithm 1** DPFMix: generating dataset via mixup

---

**Input:** Dataset  $S = \{(x_1, y_1), \dots, (x_n, y_n)\}$ , where  $x_i$  is raw data and  $y_i$  is the one-hot label, feature extractor with parameter  $f_1(\theta_1, \cdot)$ , mixup degree  $m$ , noise scale  $\sigma_x, \sigma_y$ ,  $l_2$  norm clipping bound for input and label  $C_x, C_y$ , output dataset size  $T$ .

**Output:** DP feature dataset  $S_{DP}$  for publishing

**for**  $t = 1$  **to**  $T$  **do**

**subsampling:** Select a subset of the original dataset with Poisson subsampling at rate  $p = m/n$  Definition B.3 in Appendix B.2. Create an index set  $I_t = \{i \in [n] : a_i = 1\} \subset \{1, \dots, n\}$ .

**for**  $i \in I_t$  **do**

        Extract feature:  $x_i^{(t)} = f_1(\theta_1, x_i)$

        Clip feature:  $x_i^{(t)} = x_i^{(t)} / \max(1, \|x_i^{(t)}\|_2 / C_x)$

        Clip label:  $y_i^{(t)} = y_i^{(t)} / \max(1, \|y_i^{(t)}\|_2 / C_y)$

**end for**

    Average and perturb:

$$\bar{x}_t = \frac{1}{m} \sum_{i \in I_t} x_i^{(t)} + \mathcal{N}(0, (\frac{C_x}{m} \sigma_x)^2 I)$$

$$\bar{y}_t = \frac{1}{m} \sum_{i \in I_t} y_i^{(t)} + \mathcal{N}(0, (\frac{C_y}{m} \sigma_y)^2 I)$$

$$S_{DP} = S_{DP} \cup \{(\bar{x}_t, \bar{y}_t)\}$$

**end for**

---

namely model inversion attack, and membership inference attack. Having the advantages above, DPFMix is promising in real-world applications for differentially private data release with a tight privacy budget.

## 2 Random Feature Mixup with Gaussian Differential Privacy

In this section, we will introduce the data generation by random mixup of features and its privacy analysis with Gaussian Differential Privacy.

Algorithm 1 summarizes our mechanism to generate differentially private datasets via random feature mixup, called DPFMix here. To generate one sample in the DP dataset, DPFMix will first use the Poisson sampling technique with sample rate  $\frac{m}{n}$  to get a subset of data. Then extract features of the samples. Finally, DPFMix conducts clipping, averaging, and perturbing to both features and labels. This process is repeated  $T$  times so that the size of the DP feature dataset is  $T$ . Hyper-parameters including  $m, T, C_x$ , and  $C_y$  are introduced. The most important one is the mixup degree  $m$  which we will show to be the key for maximizing the utility.  $C_x$  and  $C_y$  are used to control the sensitivity of input data and label respectively. When building classification models, one problem is that  $\bar{y}$  is not a probability vector since each element of  $\bar{y}$  might go beyond the range of  $[0, 1]$  and its  $\ell_1$ -norm is not always 1. So, we first clip the negative part of  $\bar{y}$  and use the generalized KL-divergence as loss function. The details are shown in Appendix D.

The remaining of this section shall focus on the following three key elements: Gaussian Differential Privacy, Poisson subsampling scheme, and the feature mixup.

**Gaussian Differential Privacy:** Algorithm 1 contains subsampling and composition laws which are the main concerns for DP analysis. However, it is well-known that  $(\epsilon, \delta)$ -DP framework is not tight for compositions. To overcome this issue, (Dong et al., 2021) introduced a new framework of  $f$ -DP which is tight in compositions whose asymptotic limits converge to a canonical Gaussian Differential Privacy (GDP). Here we adopt this  $f$ -DP framework with GDP limit that enables us a simple analysis of the error bound in the next section.

In the  $f$ -DP framework (Dong et al., 2021), function  $f : [0, 1] \rightarrow [0, 1]$  is convex, continuous, non-increasing, and  $0 \leq f(x) \leq 1 - x$ , which provides a lower bound of the trade-off between Type I and Type II error under a hypothesis test of identifying two neighboring datasets  $S$  and  $S'$ . Hence  $f$  is called the *trade-off* function. Composition laws of  $f$ -DP is closed under such trade-off functions and thus is tight that can not be improved in general. However, evaluating the exact composition in  $f$ -DP framework is computationally hard. Fortunately the asymptotically limit of compositions of  $f$ -DP converges to GDP with one parameter  $\mu$  which is easy to compute. GDP is a single-parameter family as a special class of  $f$ -DP and (Dong et al., 2021; Bu et al., 2020) show that GDP provide tight approximation of even finite compositions, e.g. in stochastic gradient methods. Here, we also find such approximations provide accurate results DPFMix even when  $T$  is not very large, see Appendix C.1.4 Figures 5 and 6. The systematic introduction about  $f$ -DP framework and GDP are left in Appendix B to make this paper self-contained. Here, we just state the following key theorem that Algorithm 1 meets the framework of  $f$ -DP whose asymptotic limit as  $T \rightarrow \infty$  is GDP.

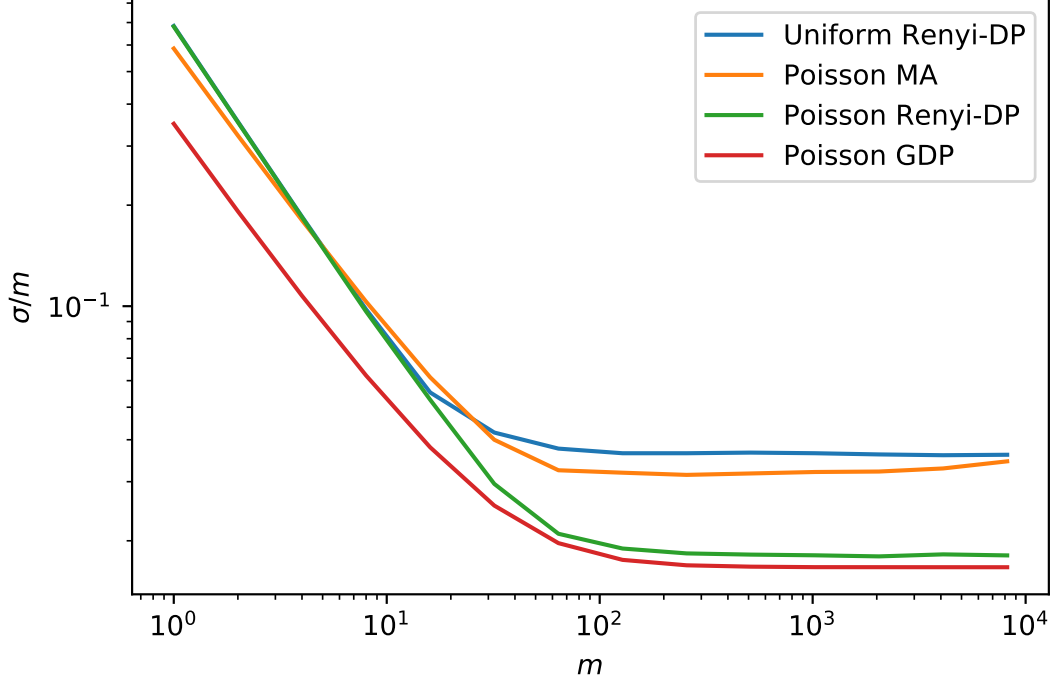


Figure 1: Comparison of noise injected to achieve  $(1, 10^{-5})$ -DP by different privacy accountants.

**Theorem 2.1.** *Algorithm 1 is  $\min\{f, f^{-1}\}^{**}$ -DP with*

$$f = \left( \frac{m}{n} G \sqrt{\frac{1}{\sigma_x^2} + \frac{1}{\sigma_y^2}} + \left(1 - \frac{m}{n}\right) Id \right)^{\otimes T}, \quad (1)$$

where  $G_\mu(\alpha) := \Phi(\Phi^{-1}(1 - \alpha) - \mu)$  and  $\Phi$  is the Gaussian cumulative distribution function. Moreover, if  $m\sqrt{T}/n \rightarrow \nu$  for a constant  $\nu > 0$  as  $T \rightarrow \infty$  Algorithm 1 is asymptotically  $\mu$ -GDP with

$$\mu = \nu \sqrt{e^{1/\sigma_x^2 + 1/\sigma_y^2} - 1}. \quad (2)$$

Its proof is left in Appendix C.1. To compare with other DP accountants, we need to transform  $\mu$ -GDP to some  $(\epsilon, \delta)$ -DP. The following result by Dong et al. (2021) shows that  $\mu$ -GDP corresponds to an infinite collection of  $(\epsilon, \delta)$ -DP.

**Lemma 2.2.** (Corollary 1 in Dong et al. (2021)) *A mechanism is  $\mu$ -GDP if and only if it is  $(\epsilon, \delta(\epsilon))$ -DP for all  $\epsilon \geq 0$ , where*

$$\delta(\epsilon) = \Phi\left(-\frac{\epsilon}{\mu} + \frac{\mu}{2}\right) - e^\epsilon \Phi\left(-\frac{\epsilon}{\mu} - \frac{\mu}{2}\right).$$

Finally, we give a comparison of different subsampling schemes and accountants. Under typical setting of DPFMix where  $T = n = 50000$ ,  $\epsilon = 1$ ,  $\delta = 10^{-5}$ , and  $\sigma_x = \sigma_y$ , we show the noise  $\sigma/m$  vs.  $m$ , injected by “Uniform RDP”, which is used in (Lee et al., 2019), “Poisson MA” Abadi et al. (2016), “Poisson RDP” (Zhu & Wang, 2019) and “Poisson GDP” (ours) in Figure 1. We can see that our analysis uses the smallest noise for all  $m$  and is thus the tightest.

**Poisson sampling:** In Algorithm 1, we select each sample independently with probability  $\frac{m}{n}$ , which is named Poisson sampling in Zhu & Wang (2019) (See Definition B.3). We choose the Poisson sampling scheme instead of the the Uniform sampling (See Definition B.4), which is used in Lee et al. (2019) for two reasons. First, Poisson sampling scheme enjoys a tighter privacy analysis for DPFMix. Theorem 6 in (Zhu & Wang, 2019) shows there is a lower bound for  $\epsilon$  under the Uniform sampling scheme. While (Wang et al., 2019) proves such lower bound is the upper bound for Gaussian mechanism when we switch to Poisson sampling. That shows the Poisson sub-sampling scheme should be at least as tight as Uniform sub-sampling. Second, the error analysis of DPFMix under Poisson sampling scheme could be simplified. The mixup process can be described as left multiplying  $M \in \mathbb{R}^{T \times n}$  by the original dataset matrix.

Under the Poisson sampling scheme, each element of  $M$  is an i.i.d. Bernoulli random variable that takes value  $\frac{1}{m}$  with probability  $\frac{m}{n}$  and 0 with probability  $1 - \frac{m}{n}$ . So, one can exploit the random matrix theory [Bai & Yin \(1993\)](#) to characterize the extreme eigenvalues of  $M$  that is crucial to optimize the mixup degree in the next section. In contrast, elements of  $M$  under the Uniform sampling scheme are correlated. Another benefit of Poisson sampling is it offers a closed-form expression for DP noise and  $\mu$  when measuring privacy with  $\mu$ -GDP.

**Feature mixup:** In practice, we find that mixup at the pixel level will cause severe utility decay when  $m$  is large even no DP noise is injected and this is one of the main reasons for the low utility of DPMix [Lee et al. \(2019\)](#). In DPFMix, mixup happens at the feature level. We observed that although the utility decay caused by increasing  $m$  still exists, it can be alleviated to a large extent. Moreover, we can benefit from powerful feature extractors, e.g. self-supervised learning, and only build linear classifiers on the DP feature dataset so that alleviate the overfitting problem of neural networks. Note that DPMix can be viewed as a special case of DPFMix using an identity mapping as the feature extractor, so our GDP privacy analysis is also an generalization for DPMix.

### 3 Optimizing the Mixup Degree

In this section, we focus on the utility of DPFMix and how to maximize it with optimal  $m$ . ([Lee et al., 2019](#)) observed there exists a “sweet spot”  $m^*$ , which can maximize the utility of DPMix. However, limited theoretical supports on this finding are given. In this section, we will show in a simple yet classical example that such a favorable choice of  $m$  does exist. Specifically, we show that for the regression model, the  $\ell_2$  error of the least square estimator based on DP protected dataset will follow a first decrease and then increase trend with respect to  $m$ , which means the utility will have an increase and then decrease trend. A similar phenomenon can be found empirically on more general models as shown in the Section 4. Interestingly, for the regression model, such choice on the order of  $m$  is exactly the same as the favorable choice of [Theorem 2.1](#), which uses  $\mu$ -GDP to approximate the exact  $f$ -DP. That suggests we could achieve the best utility and tight privacy guarantee simultaneously by finding the optimal  $m$ .

#### 3.1 Main Results

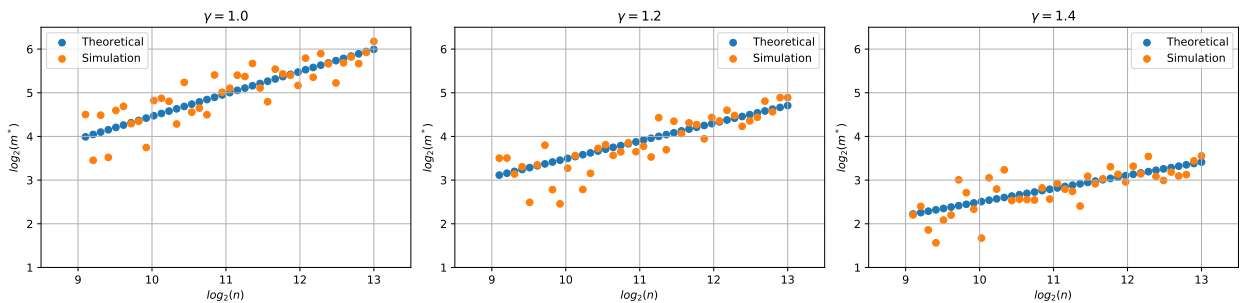


Figure 2: The figures show how  $m^*$  changes with different  $\gamma$  and  $n$ . We can verify the theoretical predicted  $m^*$  has a linear relationship in this log-log plot and the simulation results are close to the theoretical ones.

In this section, we will use the classical regression model as an example, to give a theoretical analysis that shows, there exists an optimal  $m$  that maximizes the utility of DPFMix. Consider regression model defined by

$$y = X\beta^* + \varepsilon,$$

where  $X \in \mathbb{R}^{n \times p}$  is the design matrix satisfying  $\lambda_{\min} < \text{eigen} \left( \frac{X^T X}{n} \right) < \lambda_{\max}$  for some  $\lambda_{\min}, \lambda_{\max} > 0$ ,  $\beta^* \in \mathbb{R}^p$  is the true regression parameter,  $\varepsilon \in \mathbb{R}^n$  is the i.i.d. mean zero Gaussian noise with variance  $\sigma^2$  and  $y \in \mathbb{R}^n$  is the response vector.

Let  $\tilde{X}, \tilde{Y}$  be the dataset generated after mixing up the features and adding DP noise, i.e.

$$\begin{aligned} \tilde{X} &= MX + E_X, \\ \tilde{y} &= My + E_Y, \end{aligned}$$

where  $M \in \mathbb{R}^{T \times n}$  is the random mixup matrix,  $E_X \in \mathbb{R}^{T \times p}$ ,  $E_Y \in \mathbb{R}^{T \times 1}$  are the random DP-noise matrices with their elements being i.i.d. Gaussian random variables respectively as defined in [Lemma C.3](#). Here, for simplicity we denote  $C_X = \frac{C_x \sqrt{\lambda^2 + 1}}{\lambda}$  and  $C_Y = C_y \sqrt{\lambda^2 + 1}$ , where  $\lambda := \sigma_y / \sigma_x$ .

Our target is to give an analysis on the  $\ell_2$  loss of the estimator for  $\beta^*$  based on  $\tilde{X}, \tilde{Y}$ . Consider the well-known least square estimator  $\tilde{\beta}$  given by

$$\tilde{\beta} = [\tilde{X}^T \tilde{X}]^{-1} \tilde{X}^T \tilde{y}.$$

We give the following theorem on the error of the least square estimator, i.e.  $\|\tilde{\beta} - \beta^*\|_2$ .

**Theorem 3.1.** *Let  $n, T$ , and  $m$  satisfy  $\frac{mT}{n^2} \rightarrow 0$ , and  $\frac{n}{T} \rightarrow \alpha$  for some  $0 \leq \alpha < 1$  when  $n \rightarrow \infty$ . Then there holds*

$$\begin{aligned} & \|\tilde{\beta} - \beta^*\|_2, \\ & \leq \frac{2C_X \|\beta^*\|_2 + 2C_Y}{\sqrt{\lambda_{\min}}(1 - \sqrt{\alpha})} \frac{1}{\sqrt{\frac{m(n-m)}{n} \ln\left(1 + \frac{\mu^2 n^2}{m^2 T}\right)}} + \dots \\ & \dots + \frac{2\sigma\sqrt{p} \ln n}{\sqrt{n}} \frac{(1 + \sqrt{\alpha})\sqrt{\lambda_{\max}}}{(1 - \sqrt{\alpha})\sqrt{\lambda_{\min}}}, \end{aligned} \quad (3)$$

with probability one when  $n \rightarrow \infty$ .

The proof of Thm. 3.1 is in Appendix H, based on a random matrix theoretical characterization of extreme eigenvalues of  $M^T M$ , etc.

To find an optimal rate of mixup degree  $m^*$  such that the right hand side of Eq. (3) is minimized, consider  $T = O(n^\gamma)$  with some  $1 \leq \gamma < 2$  and  $m = O(n^c)$  for  $0 \leq c < 2 - \gamma$ , then the upper bound in Eq. (3) becomes

$$\begin{cases} O\left(n^{-\frac{c}{2}} \ln^{-\frac{1}{2}}\left(n^{2-\gamma-2c}\right)\right), & 0 \leq c < \frac{2-\gamma}{2}, \\ O\left(n^{-\frac{2-\gamma}{4}}\right), & c = \frac{2-\gamma}{2}, \\ O\left(n^{-\frac{2-\gamma-c}{2}}\right), & \frac{2-\gamma}{2} < c < 2 - \gamma. \end{cases}$$

The optimal  $c^* = \frac{2-\gamma}{2}$  which the upper bound above leads to  $m^* = O\left(n^{\frac{2-\gamma}{2}}\right) = O\left(\frac{n}{\sqrt{T}}\right)$ . In this case the GDP requirement on sample rate as mentioned in Theorem 2.1,  $\frac{m\sqrt{T}}{n} = O(1)$ , is further satisfied. In summary, the reasoning above gives the following corollary.

**Corollary 3.2.** *Let  $n, T$  and  $m$  satisfy  $T = O(n^\gamma)$  for some  $1 \leq \gamma < 2$ , and  $\frac{mT}{n^2} \rightarrow 0$ . Then  $m^* = O\left(\frac{n}{\sqrt{T}}\right) = O\left(n^{\frac{2-\gamma}{2}}\right)$  is the optimal order of  $m$  that minimize right hand side of Eq. (3).*

Such a rate is tight in the simulation below and improves the result in Lee et al. (2019).

## 3.2 Simulation and Discussion

In this section, we use simulation experiments to validate our theoretical result that  $m^* = O\left(n^{\frac{2-\gamma}{2}}\right)$ . Let  $X \in \mathbb{R}^{n \times 100}$  and each row of  $X$  is sampled from  $\sim \mathcal{N}(0, \Sigma_X)$ , where  $\Sigma_X$  is the covariance matrix and  $\Sigma_{X_{i,j}} = 0.3^{|i-j|}$ . We sample  $\beta \in \mathbb{R}^{100 \times 1}$  from  $\sim \mathcal{N}(0, I)$ . Let  $Y = X\beta + \epsilon$  and each element  $\epsilon_i \sim \mathcal{N}(0, 1)$ . For DPFMix, we set  $T = 2n^\gamma$ , and  $\mu = 2$ . We choose  $C_x = 14$  and  $C_y = 36$  such that the clipping operation rarely takes effect. We run simulate experiments with different  $n$  and  $\gamma$  and compare the optimal  $m^*$  from simulation and Theorem 3.1. The results are shown in Figure 2, and we choose  $\log_2 n$  as x-axis and  $\log_2 m^*$  as the y-axis. Therefore, if  $m^* = O\left(n^{\frac{2-\gamma}{2}}\right)$ , a linear relationship between  $\log_2 m^*$  and  $\log_2 n$  with slope  $\frac{2-\gamma}{2}$  should be observable. We plot the simulation results and theoretical results predicted by Theorem 3.1 in Figure 2. One can see the simulation results are close to the theoretically predicted ones with a linear slope close to  $\frac{2-\gamma}{2}$ .

## 3.3 Comparison with Theorem 2 in Lee et al. (2019)

In Lee et al. (2019), a training MSE bound is provided with the help of convergence theory of SGD by taking  $\mathbb{E}[M^T M] = I/(mn)$  and  $m = o(n)$ , which ignores the random matrix effect of  $M$ . Theorem 2 in Lee et al. (2019) states that given  $T$ , the training MSE of a linear regression model is a monotonically increasing function of  $\sigma_x^2, \sigma_y^2$  both of which are decreasing as  $m$  increase. Based on this observation, they suggest to choose the maximal  $m = n$  for utility maximization since  $\sigma_x^2, \sigma_y^2$  are minimized when  $m = n$ . We get similar results for  $\|\tilde{\beta} - \beta^*\|_2$  when  $m \ll O\left(n^{\frac{2-\gamma}{2}}\right)$ . However, when  $m \gg O\left(n^{\frac{2-\gamma}{2}}\right)$  we see that  $\|\tilde{\beta} - \beta^*\|_2$  will increase and the utility will decay, which is different from Theorem 2 of Lee et al. (2019). This is because that the analysis there relies on the assumption  $m \ll n$  and if it is not satisfied, the random matrix effect of  $M$  can not be ignored. In fact, Theorem 3.1 here shows that the random matrix effect on the extreme eigenvalue distributions of  $M^T M$  is indispensable to find optimal  $m^*$ .

Table 1: DPMix’s test accuracy (%) of P-GDP and U-RDP schemes.

	MNIST		CIFAR10	
	U-RDP	P-GDP	U-RDP	P-GDP
$\epsilon = 1$	20.40±6.04	79.19±0.38	10.00±0.00	24.36±1.25
$\epsilon = 2$	47.63±4.24	82.71±1.33	14.33±3.77	30.37±1.30
$\epsilon = 4$	67.33±4.84	84.09±0.70	20.92±1.59	31.97±0.71
$\epsilon = 8$	73.75±2.17	85.71±0.28	25.13±1.11	31.89±0.94

## 4 Experiments

In this section, we conduct extensive experiments on DPFMix. First, we study the utility improvement of better privacy accountants in Section 4.2. We show that the Poisson sub-sampled GDP scheme could help reduce the DP noise and improve the utility compared with the Uniform sub-sampled RDP scheme used in Lee et al. (2019). The advantage of GDP becomes greater when the privacy budget is tighter.

Then in Section 4.3 we show two problems of pixel mixup and how feature mixup solves them. On the one hand, mixup at pixel level even without DP noise will suffer from severe utility decay when  $m$  is large, while feature mixup without noise has much smaller utility decay. Moreover, pixel mixup can not benefit from larger models, and using larger models will cause more severe overfitting and utility decay. On the other hand, feature mixup allows using larger models as feature extractors and only building a linear classifier on the DP features, which can alleviate the overfitting problem and take advantage of larger models at the same time. By solving the two problems, DPFMix achieves much better utility than DPMix.

In Section 4.4, we study the stability of DPFMix to hyper-parameters since the extensive search of hyper-parameters might be infeasible when dealing with private data. We first let  $\sigma_y = \lambda\sigma_x$  and studied how to balance DP noise on features and labels. With this we verified the existence of “sweet spot” mixup degree that could achieve the best utility for classification models. After a grid search, one could set  $m = 64$  and  $\lambda = 1$  in the following experiments to achieve a comparable utility with the optimal one. With this setting, Section 4.5 compares DPFMix with other private data release algorithms with a clear advantage in utility.

### 4.1 Experiment Setup

Three widely used datasets are selected: MNIST, CIFAR10, and CIFAR100. A detailed description of datasets will be shown in Appendix E.1. Since all datasets have similar size, for  $(\epsilon, \delta)$ -DP we set  $\delta = 10^{-5} \approx 1/n$  and show utility under with different  $\epsilon$  from 1 to 8. Unless stated otherwise, we report the mean and standard deviation of the accuracy of the last epoch over five independent experiments. In the experiments, we test two kinds of mixup strategies, input pixel mixup (DPMix) and feature mixup (DPFMix). We also introduce three baselines, including Non-private (NP) baseline, DPPro Xu et al. (2017), and P3GM Takagi et al. (2021). The details of the experiment setting and models are listed in Appendix E.3. Note that for DPFMix, we only train a linear classifier on the released features.

### 4.2 Improvements from GDP with Poisson Sampling

As shown in Figure 1, GDP with Poisson sampling will lead to smaller noise for a given privacy budget. Here we study the improvement of utility with smaller noise. We compare DPMix with Uniform sub-sampled Renyi-DP (U-RDP) and DPMix with Poisson sub-sampled GDP (P-GDP) in Table 1. The detailed settings are listed in Appendix E.3. We report the best accuracy with optimal  $m^*$ , since  $m^*$  might be different for different privacy accountants. We can see that in all cases, DPMix P-GDP is better than DPMix U-RDP. In particular, the advantage of P-GDP becomes larger when the privacy budget is tighter. For example, test accuracy of CIFAR10 of U-RDP with  $\epsilon = 1$  is closed to random guess, while P-GDP could still achieve test accuracy of 25.12%.

### 4.3 Improving Utility via Feature Mixup

In this section, we will show DPMix suffers from utility decay caused by input mixup and overfitting to DP noise. Then we show DPFMix, which uses feature extraction and mixup, may solve both of these problems.

**Utility decay caused by input mixup.** DPMix suffers from input mixup with large  $m$ . First, let’s focus on the utility without noise (denoted as  $\sigma = 0$ ). In Figure 3, we show the effect of  $m$  on DPMix and DPFMix. As  $m$  increases, the noise-free performance of DPMix drops quickly. That shows the information for classification can be damaged by mixing too many samples. While for DPFMix, although its utility also has a decreasing trend when we increase  $m$ , the utility decay is not as serious as the decay of DPMix. That shows feature mixup preserves more information for classification than input mixup at pixel level.

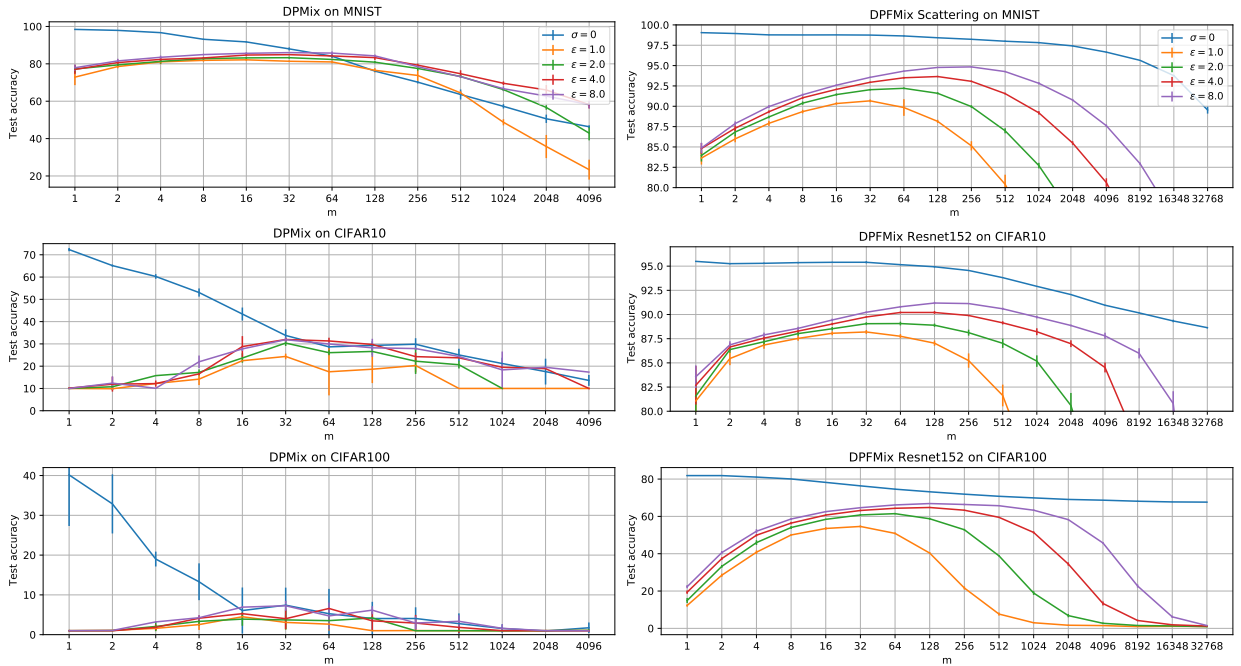


Figure 3: These figures show how utility changes w.r.t.  $m$  for DPMix of input mixup and DPFMix of feature mixup. Optimal  $m^*$  and sweet spots vary as privacy budget changes.

Table 2: CIFAR10 test accuracy (%) of DPMix and DPFMix with different models. We show the convergence test accuracy before “+” and the improvement if we reporting best accuracy during training after “+”. Due to page limits, we leave results with  $\epsilon = 1, 2, 4$  to Appendix Table 6.

	$\epsilon = 8$	NP
DPMix CNN	31.89+3.01	79.22
DPMix ResNet-50	15.52+16.19	94.31
DPMix ResNet-152	15.35+15.31	95.92
DPFMix ResNet-50	80.75+0.04	94.31
DPFMix ResNet-152	90.83+0.04	95.92

**Utility decay caused by overfitting.** Then, we analyze the model built on the mixed samples. One may notice that the 5-layer CNN (CNN) used in (Lee et al., 2019) is quite small with about 0.53M parameters. One intuitive solution to improve its utility is using larger networks, which have better non-private utility. Unfortunately, as we show in Table 2, the gap between the best test accuracy during training and final test accuracy becomes larger when we use ResNets, which suggests severe overfitting happens. Moreover, larger networks lead to a degeneration of utility. We give two explanations for the phenomena. First, the information for classification is already destroyed by pixel mixup. Therefore, larger models can not learn more from the DP dataset. Second, powerful models tend to overfit the DP noise so that have weaker convergence test accuracy. While in the DPFMix, we apply feature extraction to raw images so that we could take advantage of large pre-trained models. Then, building linear classifiers, which are less likely to overfit the noises, is enough to achieve decent utility. In Table 2, we show that the convergence utility of DPFMix is closed to the best one during the whole training process. That suggests DPFMix with linear classifiers does not overfit the DP noise too much like CNNs in DPMix. Therefore, we do not rely on the assumption of a validation dataset to do early stopping, which is used in (Lee et al., 2019) and might be not feasible when data is private.

#### 4.4 Hyper-parameter Tuning of DPFMix

**Keeping balance between noise on features and labels by tuning  $\lambda$ :** The detailed grid search results are left in Appendix Figure 7. There are different optimal  $\lambda$  for each setting. MNIST and CIFAR10 prefers  $\lambda \in [1, 4]$ . While CIFAR100 dataset prefers  $\lambda \in [0.5, 2]$  since CIFAR100 has more categories and will be more sensitive to the noise on labels. When searching optimal  $\lambda$  is not feasible in practice, we think  $\lambda \in [1, 2]$  could be a good choice. For example, comparing with optimal settings, the maximal loss on test accuracy is 1.49%, 1.08% and, 0.46% for MNIST, CIFAR10, and, CIFAR100 respectively when we set  $\lambda = 1$ .

**Choosing mixup degree  $m$ :** We conduct a grid search for finding optimal  $m$  with  $\lambda = 1$  and the results are shown in Figure 3. There are three key observations. First, in all cases including DPMix and DPFMix, the utility has

Table 3: The table shows test accuracy (%) of different algorithms on MNIST, CIFAR10, and CIFAR100. For DPMix, we show the best test accuracy with  $m^*$ .

	MNIST				CIFAR10			CIFAR100		
	DPPro	P3GM	DPMix	DPFMix	DPPro	DPMix	DPFMix	DPPro	DPMix	DPFMix
$\epsilon = 1$	11.35±0.00	79.53±0.22	82.16±0.54	<b>89.82±1.04</b>	15.49±0.94	24.36±1.25	<b>87.74±0.16</b>	1.51±0.19	4.5±0.47	<b>50.80±0.74</b>
$\epsilon = 2$	11.35±0.01	81.57±0.12	83.28±0.53	<b>92.20±0.11</b>	26.49±2.50	30.37±1.30	<b>89.01±0.15</b>	2.13±0.55	4.2±0.46	<b>60.35±0.31</b>
$\epsilon = 4$	11.35±0.02	83.23±0.40	84.90±0.26	<b>93.50±0.11</b>	54.16±3.20	31.97±0.71	<b>90.21±0.13</b>	3.64±1.00	6.58±0.23	<b>64.53±0.20</b>
$\epsilon = 8$	17.25±4.00	84.21±0.06	86.00±0.28	<b>94.32±0.07</b>	76.16±1.97	31.89±0.94	<b>90.83±0.09</b>	2.50±8.76	7.26±1.25	<b>66.35±0.32</b>

an increasing-decreasing trend and there is an optimal  $m^*$  that can maximize the utility. Second, for the same task, smaller privacy budgets tend to have smaller optimal  $m$ . Third, when tuning  $m$  is not feasible, setting an empirical value for  $m$  still works and will not lose too much utility. From Figure 3, we can see for all three datasets, the  $m^*$  is between 32 and 256. We may choose  $m = 64$  to be an empirical choice. Then the maximal loss on test accuracy is 0.74%, 0.46% and, 3.40% for MNIST, CIFAR10, and, CIFAR100 respectively and that should be acceptable.

## 4.5 Utility Comparisons with Other methods

We compare the utility of DPFMix with DPPro (Xu et al., 2017), P3GM (Takagi et al., 2021), and DPMix Lee et al. (2019). Here we only show DPFMix with  $m = 64$ ,  $\lambda = 1$ , and the utility of DPFMix could be further improved if we adjust  $m$  and  $\lambda$  for each setting. MNIST and CIFAR10/100 test accuracy is shown in Table 3. We can see in all cases, DPFMix outperforms others by a large margin. DPPro has weaker utility since it is not suitable for image data, which usually consists of more than one thousand dimensions. Although Takagi et al. (2021) shows P3GM could generate samples closed to the original ones, machine learning models built on these synthetic data have a weaker utility. The above results show the advantage of DPFMix and suggest DPFMix is a proper algorithm for publishing data for building machine learning models when dealing with high-dimensional image data.

## 5 Attacking DPFMix

In this section, we will explore model inversion attack and membership inference against DPFMix. The attacking results show that our DPFMix offers much better protection compared to the algorithms without DP guarantees.

### 5.1 Model Inversion Attack

DPFMix gives a tight DP guarantee to the feature dataset. However, we still want to know whether one can recover the original data from the released features. Model Inversion Attack (MIA) (He et al., 2019) has successfully recovered the raw data from the features released by split learning in both white-box and black-box settings. We modified the white-box attack in (He et al., 2019) to attack DPFMix. The details about the attack algorithm and more attacking results are shown in Appendix G due to page limit. The visualization results are shown in Figure 4.

The protection of DPFMix comes from three parts. First, model inversion attacks on very deep models are weak, and inverting ResNet-152 is quite hard in practice (See Appendix Figure 8 for MIA on ResNet-152 features). However, this protection can be weak if feature extractors are small and shallow, for example, when  $m = 1$  and  $\sigma = 0$ , MIA could perfectly recover the raw images from the ScatteringNet Oyallon & Mallat (2015) features. Second, the mixup operation makes the feature noisy and contains information from different images. The recovered images look like averaged ones and when  $m$  is large enough, for example,  $m = 64$ , the recovered images look entangled and individual information is hidden. However, when  $m$  is small, for example,  $m \leq 4$ , we can still recognize digits and objects from the entangled images. Finally, DP gives us a unified trade-off between  $m$  and noise scale and makes sure the noise is strong enough to perturb any individual feature. For both  $\epsilon = 1$  and  $\epsilon = 8$  cases, all the recovered images look like pure noise with some random pattern, which might be caused by the Gaussian noise and total variation prior. This protection can be reliable even when the privacy budget is quite loose in theory.

### 5.2 Membership Inference

In this section, we conduct membership inference on the CIFAR100 dataset with ResNet-152 features. Although many membership attack algorithms are proposed in Shokri et al. (2017); Salem et al. (2018); Choquette-Choo et al. (2021); Jayaraman et al. (2021), we follow (Yeom et al., 2018a; Salem et al., 2018) and focus on two algorithm-independent metrics: training testing accuracy gap (GAP) and instance loss-based AUC (AUC). In an ideal case when no membership leakage, GAP should be 0 and AUC should be 0.5. We follow the setting with fix  $m = 64$  and  $\lambda = 1$ .

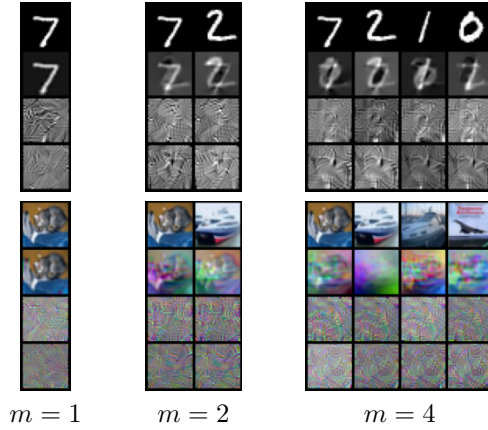


Figure 4: Attacking from features of ScatteringNet on MNIST and CIFAR10 dataset. The first row corresponds to raw images, and the following three correspond to recovered images by MIA with  $\sigma = 0$ ,  $\epsilon = 8$ , and  $\epsilon = 1$  respectively. Due to the limited space, we leave  $m = 8, 16, 32, 64$  to the appendix Figures 9 and 10.

The results are shown in Table 4. We found that non-private models built on ResNet-152 features are likely to overfit the training data. The AUC and GAP could reach 0.5735 and 9.42%, which is significantly larger than the perfect case. Then we turn to DPFMix with different settings.  $\sigma = 0$  represents we do not inject DP noise to the mixed features of  $m = 64$  samples. DPFMix with  $\sigma = 0$  reduces the AUC and GAP a lot compared with the non-private setting. This experiment shows the mixup operation could induce membership protection to some degree. Then we find the membership leakage could be further reduced when we use DPFMix with DP guarantees. Even when  $\epsilon = 8$ , which offers very loose protection in theory, DPFMix could make the membership leakage very close to perfect protection case. These empirical results show DPFMix should be used when we do care about membership protection in practice.

Table 4: Membership inference on CIFAR100 dataset.

	Test Acc	AUC	GAP
Non-private	84.45±0.02	0.5735±0.0000	9.42±0.02
DPFMix $\sigma = 0$	74.57±0.04	0.5160±0.0002	2.49±0.09
DPFMix $\epsilon = 8$	66.35±0.32	0.5075±0.0004	1.08±0.20
DPFMix $\epsilon = 4$	64.53±0.20	0.5065±0.0004	0.83±0.06
DPFMix $\epsilon = 2$	60.35±0.31	0.5061±0.0006	1.26±0.44
DPFMix $\epsilon = 1$	50.80±0.74	0.5033±0.0015	0.57±0.33

## 6 Conclusion

In this paper, we try to optimize DPMix with recent advances in privacy-preserving machine learning. We first give a quantitative characterization of optimal  $m^*$ , which is the key to optimizing the utility of DPMix. Then we show feature extractors like self-supervised learning models could boost the utility of DPMix. We name it DPFMix and show DPFMix is not sensitive to hyper-parameter settings and could defense model inversion attacks and membership inference. All the results show the potential of DPFMix in practice. We hope our work inspires more study and applications on the problem of privacy-preserving high-dimensional data releasing, which will be an increasingly important topic in machine learning community.

## References

- Abadi, M., Chu, A., Goodfellow, I., McMahan, H. B., Mironov, I., Talwar, K., and Zhang, L. Deep learning with differential privacy. In *Proceedings of the 2016 ACM SIGSAC conference on computer and communications security*, pp. 308–318, 2016.
- Acs, G., Melis, L., Castelluccia, C., and De Cristofaro, E. Differentially private mixture of generative neural networks. *IEEE Transactions on Knowledge and Data Engineering*, 31(6):1109–1121, 2018.
- Apple, D. P. T. Learning with privacy at scale. Technical report, Apple, 2017.
- Bai, Z. D. and Yin, Y. Q. Limit of the smallest eigenvalue of a large dimensional sample covariance matrix. *The Annals of Probability*, 21(3):1275–1294, 1993. ISSN 00911798. URL <http://www.jstor.org/stable/2244575>.

- Bu, Z., Dong, J., Long, Q., and Su, W. J. Deep learning with gaussian differential privacy. *Harvard data science review*, 2020(23), 2020.
- Carlini, N., Deng, S., Garg, S., Jha, S., Mahloujifar, S., Mahmood, M., Song, S., Thakurta, A., and Tramer, F. An attack on instahide: Is private learning possible with instance encoding? *arXiv preprint arXiv:2011.05315*, 2020.
- Chen, T., Kornblith, S., Swersky, K., Norouzi, M., and Hinton, G. E. Big self-supervised models are strong semi-supervised learners. *Advances in Neural Information Processing Systems*, 33:22243–22255, 2020.
- Chidambaram, M., Wang, X., Hu, Y., Wu, C., and Ge, R. Towards understanding the data dependency of mixup-style training, 2021.
- Choquette-Choo, C. A., Tramer, F., Carlini, N., and Papernot, N. Label-only membership inference attacks, 2021.
- Ding, B., Kulkarni, J., and Yekhanin, S. Collecting telemetry data privately. In *NIPS*, 2017.
- Dong, J., Roth, A., and Su, W. Gaussian differential privacy. *Journal of the Royal Statistical Society, Series B*, 00: 1–35, 2021. (with discussion).
- Dwork, C., McSherry, F., Nissim, K., and Smith, A. Calibrating noise to sensitivity in private data analysis. In Halevi, S. and Rabin, T. (eds.), *Theory of Cryptography*, pp. 265–284, Berlin, Heidelberg, 2006. Springer Berlin Heidelberg. ISBN 978-3-540-32732-5.
- Dwork, C., Roth, A., et al. The algorithmic foundations of differential privacy. *Foundations and Trends in Theoretical Computer Science*, 9(3-4):211–407, 2014.
- Erlingsson, Ú., Pihur, V., and Korolova, A. Rappor: Randomized aggregatable privacy-preserving ordinal response. In *Proceedings of the 2014 ACM SIGSAC conference on computer and communications security*, pp. 1054–1067, 2014.
- Frigerio, L., de Oliveira, A. S., Gomez, L., and Duverger, P. Differentially private generative adversarial networks for time series, continuous, and discrete open data. In *IFIP International Conference on ICT Systems Security and Privacy Protection*, pp. 151–164. Springer, 2019.
- Goodfellow, I. J., Shlens, J., and Szegedy, C. Explaining and harnessing adversarial examples. *arXiv preprint arXiv:1412.6572*, 2015.
- He, Z., Zhang, T., and Lee, R. B. Model inversion attacks against collaborative inference. In *Proceedings of the 35th Annual Computer Security Applications Conference*, pp. 148–162, 2019.
- Huang, Y., Song, Z., Chen, D., Li, K., and Arora, S. Texthide: Tackling data privacy for language understanding tasks. In *Proceedings of the 2020 Conference on Empirical Methods in Natural Language Processing: Findings*, pp. 1368–1382, 2020a.
- Huang, Y., Song, Z., Li, K., and Arora, S. Instahide: Instance-hiding schemes for private distributed learning. In *International Conference on Machine Learning*, pp. 4507–4518. PMLR, 2020b.
- Jayaraman, B., Wang, L., Knipmeyer, K., Gu, Q., and Evans, D. Revisiting membership inference under realistic assumptions, 2021.
- Kenthapadi, K. and Tran, T. T. Pripearl: A framework for privacy-preserving analytics and reporting at linkedin. In *Proceedings of the 27th ACM International Conference on Information and Knowledge Management*, pp. 2183–2191, 2018.
- Kenthapadi, K., Mironov, I., and Thakurta, A. G. Privacy-preserving data mining in industry. In *Proceedings of the Twelfth ACM International Conference on Web Search and Data Mining*, pp. 840–841, 2019.
- Kingma, D. P. and Ba, J. Adam: A method for stochastic optimization. In *ICLR (Poster)*, 2015.
- Lee, K., Kim, H., Lee, K., Suh, C., and Ramchandran, K. Synthesizing differentially private datasets using random mixing. In *2019 IEEE International Symposium on Information Theory (ISIT)*, pp. 542–546. IEEE, Jul 2019. ISBN 978-1-5386-9291-2. doi: 10.1109/ISIT.2019.8849381. URL <https://ieeexplore.ieee.org/document/8849381/>.
- Li, N., Qardaji, W., and Su, D. On sampling, anonymization, and differential privacy or, k-anonymization meets differential privacy. In *Proceedings of the 7th ACM Symposium on Information, Computer and Communications Security*, pp. 32–33, 2012.

- Liang, Z., Wang, B., Gu, Q., Osher, S., and Yao, Y. Differentially private federated learning with laplacian smoothing. *NeurIPS Workshop on Federated Learning for Data Privacy and Confidentiality, Vancouver, Canada, Dec. 8-14, 2019*, 2020.
- McKenna, R., Sheldon, D., and Miklau, G. Graphical-model based estimation and inference for differential privacy. In *International Conference on Machine Learning*, pp. 4435–4444. PMLR, 2019.
- McKenna, R., Miklau, G., and Sheldon, D. Winning the NIST contest: A scalable and general approach to differentially private synthetic data. *CoRR*, abs/2108.04978, 2021. URL <https://arxiv.org/abs/2108.04978>.
- McMahan, B., Moore, E., Ramage, D., Hampson, S., and y Arcas, B. A. Communication-efficient learning of deep networks from decentralized data. In *Artificial Intelligence and Statistics*, pp. 1273–1282. PMLR, 2017.
- Mironov, I. Rényi differential privacy. *2017 IEEE 30th Computer Security Foundations Symposium (CSF)*, Aug 2017. doi: 10.1109/csf.2017.11. URL <http://dx.doi.org/10.1109/CSF.2017.11>.
- NIST. 2018 differential privacy synthetic data challenge, Jan 2021. URL <https://www.nist.gov/ctl/pscr/open-innovation-prize-challenges/past-prize-challenges/2018-differential-privacy-synthetic>.
- Oyallon, E. and Mallat, S. Deep roto-translation scattering for object classification. In *Proceedings of the IEEE Conference on Computer Vision and Pattern Recognition*, pp. 2865–2873, 2015.
- Rudin, L. I., Osher, S., and Fatemi, E. Nonlinear total variation based noise removal algorithms. *Physica D: nonlinear phenomena*, 60(1-4):259–268, 1992.
- Salem, A., Zhang, Y., Humbert, M., Berrang, P., Fritz, M., and Backes, M. MI-leaks: Model and data independent membership inference attacks and defenses on machine learning models, 2018.
- Shokri, R., Stronati, M., Song, C., and Shmatikov, V. Membership inference attacks against machine learning models, 2017.
- Takagi, S., Takahashi, T., Cao, Y., and Yoshikawa, M. P3gm: Private high-dimensional data release via privacy preserving phased generative model. In *2021 IEEE 37th International Conference on Data Engineering (ICDE)*, pp. 169–180. IEEE, 2021.
- Tramer, F. and Boneh, D. Differentially private learning needs better features (or much more data). In *International Conference on Learning Representations*, 2021. URL <https://openreview.net/forum?id=YTWGvpFOQD->.
- Vepakomma, P., Gupta, O., Swedish, T., and Raskar, R. Split learning for health: Distributed deep learning without sharing raw patient data. *arXiv preprint arXiv:1812.00564*, 2018.
- Verma, V., Lamb, A., Beckham, C., Najafi, A., Mitliagkas, I., Lopez-Paz, D., and Bengio, Y. Manifold mixup: Better representations by interpolating hidden states. In *International Conference on Machine Learning*, pp. 6438–6447. PMLR, 2019.
- Wang, Y.-X., Balle, B., and Kasiviswanathan, S. P. Subsampled rényi differential privacy and analytical moments accountant. In *The 22nd International Conference on Artificial Intelligence and Statistics*, pp. 1226–1235. PMLR, 2019.
- Wasserman, L. and Zhou, S. A statistical framework for differential privacy. *Journal of the American Statistical Association*, 105(489):375–389, 2010.
- Wu, Y. and He, K. Group normalization. In *Proceedings of the European conference on computer vision (ECCV)*, pp. 3–19, 2018.
- Xie, L., Lin, K., Wang, S., Wang, F., and Zhou, J. Differentially private generative adversarial network. *arXiv preprint arXiv:1802.06739*, 2018.
- Xu, C., Ren, J., Zhang, Y., Qin, Z., and Ren, K. Dppro: Differentially private high-dimensional data release via random projection. *IEEE Transactions on Information Forensics and Security*, 12(12):3081–3093, 2017. doi: 10.1109/TIFS.2017.2737966.
- Xu, C., Ren, J., Zhang, D., Zhang, Y., Qin, Z., and Ren, K. Ganobfuscator: Mitigating information leakage under gan via differential privacy. *IEEE Transactions on Information Forensics and Security*, 14(9):2358–2371, 2019.
- Yeom, S., Giacomelli, I., Fredrikson, M., and Jha, S. Privacy risk in machine learning: Analyzing the connection to overfitting. In *2018 IEEE 31st Computer Security Foundations Symposium (CSF)*, pp. 268–282. IEEE, 2018a.

- Yeom, S., Giacomelli, I., Fredrikson, M., and Jha, S. Privacy risk in machine learning: Analyzing the connection to overfitting, 2018b.
- Yu, D., Zhang, H., Chen, W., and Liu, T.-Y. Do not let privacy overbill utility: Gradient embedding perturbation for private learning. In *International Conference on Learning Representations*, 2021a.
- Yu, D., Zhang, H., Chen, W., Yin, J., and Liu, T.-Y. Large scale private learning via low-rank reparametrization. In *International Conference on Machine Learning (ICML)*, July 2021b.
- Zhang, H., Cisse, M., Dauphin, Y. N., and Lopez-Paz, D. Mixup: Beyond empirical risk minimization. *arXiv preprint arXiv:1710.09412*, 2017a.
- Zhang, J., Cormode, G., Procopiuc, C. M., Srivastava, D., and Xiao, X. Privbayes: Private data release via bayesian networks. *ACM Trans. Database Syst.*, 42(4), oct 2017b. ISSN 0362-5915. doi: 10.1145/3134428. URL <https://doi.org/10.1145/3134428>.
- Zhang, X., Ji, S., and Wang, T. Differentially private releasing via deep generative model (technical report). *arXiv preprint arXiv:1801.01594*, 2018.
- Zhu, L. and Han, S. Deep leakage from gradients. In *Federated Learning*, pp. 17–31. Springer, 2020.
- Zhu, T., Li, G., Zhou, W., and Philip, S. Y. Differentially private data publishing and analysis: A survey. *IEEE Transactions on Knowledge and Data Engineering*, 29(8):1619–1638, 2017.
- Zhu, Y. and Wang, Y.-X. Poission subsampled rényi differential privacy. In *International Conference on Machine Learning*, pp. 7634–7642. PMLR, 2019.

## A Related Works

In this section, we some related works including Differential Privacy, differentially private data release algorithms, DPSGD, mixup, and its application to protect privacy. We also introduce two threats, namely model inversion attack and membership inference.

### A.1 Differential Privacy

$(\epsilon, \delta)$ -differential privacy [Dwork et al. \(2006\)](#) is a widely accepted rigorous definition of privacy. Under the differential privacy framework, we want to prevent attackers that want to determine whether some user exists in the private dataset by querying the dataset. Therefore, the DP mechanism needs to constrain the outputs of any query such that it will not differ a lot regardless of the existence of some user. Here is the definition of DP.

*Definition A.1.* A randomized algorithm  $M$  satisfies  $(\epsilon, \delta)$ -differential privacy if for any two neighboring datasets  $S, S'$  and any event  $E$ ,

$$P(M(S) \in E) \leq e^\epsilon P(M(S') \in E) + \delta$$

To achieve DP, we need to bound the individual impact of one record and add randomness to the mechanism by injecting Gaussian noise. Sensitivity is used to measure the worst-case individual impact of a function.

*Definition A.2.* The  $l_2$ -sensitivity  $\Delta_f$  of a function  $f$  is defined as

$$\Delta_f := \max_{S, S'} \|f(S) - f(S')\|$$

There are two appealing properties for DP. First, DP is robust to post-process, which means that any function based on the output of  $(\epsilon, \delta)$ -DP mechanism is still  $(\epsilon, \delta)$ -DP. Second, although naive composition fails to offer a tight bound, DP allows analysis privacy loss of iterated algorithms, for example, stochastic gradient descent.

However,  $(\epsilon, \delta)$ -DP framework is not flexible enough to tightly handle subsampling and compositions. Relaxations of  $(\epsilon, \delta)$ -DP including Renyi-DP [Mironov \(2017\)](#) (RDP) and GDP [Dong et al. \(2021\)](#) are proposed to tightly handle subsampling and compositions. In this paper, we choose GDP since it offers tight and closed-form privacy guarantees. A systematic introduction is given in [Appendix B](#).

### A.2 Differentially Private Data Release Algorithms

There are many research efforts devoted to this area. Here we only focus on DP data release algorithms for high dimensional data, which are related to DPFMix. For readers who are interested in the border area, the survey ([Zhu et al., 2017](#)) could offer a systematic introduction.

PrivBayes construct a noisy Bayes network to capture the joint distribution of the data. When building the Bayes network, DP noise is injected to ensure differential privacy. Then, one can sample from the Bayes network to get synthetic data with DP guarantees. DPPro ([Xu et al., 2017](#)) tried to use random projection to reduce the dimension of the features so that reduces the sensitivity of the data and avoids the curse of dimensionality. NIST-MST ([McKenna et al., 2021](#)) is the winning algorithm of Differential Privacy Synthetic Data Competition [NIST \(2021\)](#). NIST-MST first computes noisy marginals of data and utilizes Private-PGM [McKenna et al. \(2019\)](#) to estimate the joint distribution and generate a synthetic dataset. However, these methods still suffer from the curse of dimensionality. They are usually tested on tabular datasets with dozens of dimensions. DPMix ([Lee et al., 2019](#)) shows DPPro cannot work on MNIST too. ([Takagi et al., 2021](#)) shows PrivBayes ([Zhang et al., 2017b](#)) and the NIST-MST ([McKenna et al., 2021](#)) can not work on the MNIST dataset with 784 dimensions.

Some researchers also use deep generated models to create synthetic data for very high-dimensional data. The deep generated models are trained with DP guarantees so that the generated data from these models also satisfies DP. Generative Adversarial Networks (GANs) and Variational Auto Encoder (VAE) have been explored to create DP synthetic data. ([Xie et al., 2018](#)) first proposed training DP GANs for private data release. ([Zhang et al., 2018](#)) introduce parameter grouping, adaptive clipping, and warm starting to improve the training stability and convergence speed rate of DPGANs. ([Xu et al., 2019](#)) further optimize DPGANs by only injecting noise to discriminators of GANs and design an adaptive clipping strategy for gradients. ([Frigerio et al., 2019](#)) studies DPGANs for releasing different types of data from the time-series data to continuous data, and discrete data. Under the VAE framework, a simple combination of DPSGD and VAE produces noisy synthetic data. ([Acs et al., 2018](#)) conduct k-mean to group the private data and build VAEs for each group of data. However, ([Takagi et al., 2021](#)) shows DP-GM suffers from mode collapse and low utility for machine learning tasks. P3GM ([Takagi et al., 2021](#)) modifies the training procedure into two phases. P3GM first train the encoder and then train the decoder with a fixed encoder. P3GM states its advantage both theoretically and empirically. These methods using generative models aim at generating synthetic data close to the private ones and they are always evaluated with visualizations that show they are very closed to the original data. Compared with these methods, our goal is quite different. We want to release a noisy dataset for training machine

learning algorithms and, if possible, the released data should look completely noisy and do not leak any patterns of the private data.

DPMix (Lee et al., 2019) is a novel algorithm, which is different from all the methods mentioned above and has the potential to release very high-dimensional data. DPMix (Lee et al., 2019) releases noisy averaged samples as a synthetic DP dataset. Specifically, DPMix first samples a subset with  $m$  samples and then computes the average of the subset. Gaussian noise is injected to ensure DP. The averaging process is introduced to reduce the sensitivity of the operation so that the Gaussian noise could be smaller if  $m$  is larger. However, the utility of the synthetic data could decay when  $m$  is too large and there is a “sweet spot”  $m$  that could maximize its utility. Such phenomena have been observed without rigorous justification. Moreover, experiments (Lee et al., 2019) show its potential to release image data for building machine learning algorithms. In this paper, we revisit DPMix with recent progress on DP learning. In theory, we proved that there exists an optimal  $m^*$  and show  $m^* = O\left(n^{\frac{2-\gamma}{2}}\right)$  under the linear regression setting. In practice, we boost the performance by introducing feature extraction.

### A.3 DPSGD

DPSGD (Abadi et al., 2016) injects noise to the gradient during the optimization process. Specifically, in each gradient update, the instance gradient is clipped to have a bounded  $l_2$ -norm and isotropic Gaussian noise is injected so that each step satisfies DP. Composition is used to calculate the DP budget of the whole training process, which is composed of multiple gradient updates. subsampling is used for characterizing mini-batch stochastic gradient descent. Moreover, the variants of SGD can be modified to satisfy DP when the gradient is properly processed.

However, DPSGD suffers from low utility compared with SGD. There are many works that focus on boosting its utility via modifying DPSGD, including (Liang et al., 2020; Yu et al., 2021a,b). (Tramer & Boneh, 2021) propose another way to boost DP learning by using feature extraction. Specifically, Tramer & Boneh (2021) found fix feature extractions with a linear classifier outperforming end-to-end trained deep learning models with moderate privacy budgets. It suggests that differentially private learning fails to learn good feature representations and we should use better feature extractors like ScatteringNet (Oyallon & Mallat, 2015) or pre-trained networks when the dataset is not large enough. In this paper, we follow Tramer & Boneh (2021) and choose ScatteringNet (Oyallon & Mallat, 2015) and pre-trained SimCLRv2 (Chen et al., 2020) as the feature extractor.

### A.4 Mixup and Its Extension to PPML

Mixup proposed in (Zhang et al., 2017a) is a data augmentation scheme that randomly linearly interpolates images and corresponding one-hot labels. Then use the mixed data as training data. By encouraging the linear behavior of neural networks, mixup improves the generalization of different neural networks. Besides, mixup reduces the memorization of the training dataset and the success rate of fast gradient sign method (Goodfellow et al., 2015) adversarial attack. An adaptive version of mixup called AdaMixUp further improves mixup by learning mixing policies automatically from the data. (Chidambaram et al., 2021) studied the margin of mixup classifier and explained when and why mixup training have better generalization than standard training. Feature mixup is first studied in (Verma et al., 2019). Recently, researchers develop mixup-based PPML algorithms including DPMix (Lee et al., 2019), which we have introduced and InstaHide (Huang et al., 2020b).

Proposed in (Huang et al., 2020b), InstaHide shows empirical success in image classification tasks. It uses randomly weighted averaged pixels of 4 to 6 images to train neural networks. Besides, InstaHide introduces a one-time secret mask to encrypt the raw images. The authors show the connection between the one-time secret mask and the  $k$ -VECTOR-SUBSET-SUM problem which is known to be NP-complete. Then (Huang et al., 2020a) further extend InstaHide to the NLP domain. However, some researchers found InstaHide can be attacked even under the strongest setting (Carlini et al., 2020). Specifically, they recover images in the InstaHide challenge successfully. They also explore implementation flaws and undo the encryption by extracting pseudo-random number generators. That shows that InstaHide may not be a safe method in some situations.

### A.5 Attacking Algorithms

#### Model inversion attack

Model Inversion Attack against split learning is first introduced in (He et al., 2019). The goal of this attack is trying to reconstruct the original input of the model when training or inference from released intermediate features. Under the white-box attack setting, the attackers know intermediate features and the neural network with parameters. Then attackers can use regularized Maximum Likelihood Estimation (rMLE) to recover the input data. Since our DPFMix will release the mixed features, the model inversion attack is a proper attack method for DPFMix. We will modify the attack algorithm to adopt mixup setting and show we can defend this type of attack using extensive experiments.

**Membership Inference** In Membership Inference, the attackers try to infer whether a sample appears in the training set. Membership inference against machine learning models was firstly studied in (Shokri et al., 2017). The

attackers mimic the target model behavior by training several “shadow models” with the same training setting as the target model, then train a binary classification model based on shadow model outputs to predict membership. Authors of [Salem et al. \(2018\)](#) further relax the assumptions in [Shokri et al. \(2017\)](#) and propose three alternative attacking algorithms. Area Under receiver operating characteristic Curve (AUC) is also introduced in [Salem et al. \(2018\)](#) as a threshold independent metric for privacy leakage. [Yeom et al. \(2018b\)](#) introduce a metric named “membership advantage” and show its connection with DP. [Choquette-Choo et al. \(2021\)](#) introduce label only membership inference algorithms which are much easier to apply and robust to output perturbation. Recently, [Jayaraman et al. \(2021\)](#) introduced a more realistic membership inference under skewed priors. In addition to membership inference algorithms, researchers [Shokri et al. \(2017\)](#); [Yeom et al. \(2018b\)](#); [Salem et al. \(2018\)](#); [Choquette-Choo et al. \(2021\)](#) show that the success of membership inference depends on the generalization abilities of machine learning models. Empirically, a larger generalization gap will make the membership attack easier. In our membership inference experiments, we adopt generalization gap and instance loss-based AUC as two metrics for membership leakage.

## B $f$ -DP framework

In this section, we give a self-contained introduction to  $f$ -DP framework. We will first introduce the definition of  $f$ -DP and  $\mu$ -GDP. Then show how  $f$ -DP handles subsampling and composition tightly. Since computing exact  $f$ -DP can be hard when  $T$  is large, we introduce the “central limit theorem” phenomena and  $\mu$ -GDP approximation. To compare with other DP accountants, we also show the connection between  $\mu$ -GDP and  $(\epsilon, \delta)$ -DP.

### B.1 $f$ -Differential Privacy

Under the differential privacy framework, we want to prevent an attacker who is well-informed about the dataset except for one single individual from knowing the presence or absence of the unknown individual. ([Wasserman & Zhou, 2010](#)) first interprets such attack as a hypothesis testing problem:

$$H_0: \text{the true dataset is } S \quad \text{versus} \quad H_1: \text{the true dataset is } S'$$

We can defend such attack by injecting randomness so that constrain the Type I error and Type II error of the hypothesis test over all possible rejection rules  $\phi$ . Let  $P$  and  $Q$  denote the distributions of  $M(S)$  and  $M(S')$  and ([Dong et al., 2021](#)) defines the *trade-off function* between  $P$  and  $Q$  as:

$$T(P, Q) : [0, 1] \mapsto [0, 1] \\ \alpha \mapsto \inf_{\phi} \{1 - E_Q[\phi] : E_P[\phi] \leq \alpha\},$$

where  $E_P[\phi]$  and  $1 - E_Q[\phi]$  are type I and type II errors of the rejection rule  $\phi$ .  $T(P, Q)(\alpha)$  is thus the minimal type II error given type I error no more than  $\alpha$ . Proposition 2.2 in ([Dong et al., 2021](#)) shows that a function  $f$  is a trade-off function if and only if  $f$  is convex, continuous, non-increasing, and  $f(x) \leq 1 - x$  for  $x \in [0, 1]$ . Then  $f$ -DP is defined by bounding from the lower by  $f$  the trade-off function between Type I and Type II error.

*Definition B.1.* ([Dong et al., 2021](#)) Let  $f$  be a trade-off function. A (randomized) algorithm  $M$  is  $f$ -DP if:

$$T(M(S), M(S')) \geq f$$

for all neighboring datasets  $S$  and  $S'$ .

A particular case of  $f$ -DP is the  $\mu$ -Gaussian Differential Privacy (GDP) ([Dong et al., 2021](#)), which is a single-parameter family of privacy definitions within the  $f$ -DP class.

*Definition B.2.* [Dong et al. \(2021\)](#) A (randomized) algorithm  $M$  is  $\mu$ -GDP if

$$T(M(S), M(S')) \geq G_{\mu}$$

for all neighboring datasets  $S$  and  $S'$ , where  $G_{\mu}(\alpha) = \Phi(\Phi^{-1}(1 - \alpha) - \mu)$  and  $\Phi$  is the Gaussian cumulative distribution function.

Intuitively, GDP is to  $f$ -DP as normal random variables to general random variables. Let  $G_{\mu} = T(\mathcal{N}(0, 1), \mathcal{N}(\mu, 1))$  be the trade-off function. Intuitively, GDP uses the difficulty of distinguishing  $\mathcal{N}(0, 1)$  and  $\mathcal{N}(\mu, 1)$  with only one sample to measure the difficulty of the above attack. Therefore larger  $\mu$  means easier to distinguish whether a sample is in the dataset and larger privacy leakage. The most important property of GDP, as will be introduced below, is a central limit theorem that the limit of composition of many “private” mechanisms converge to GDP.

## B.2 Subsampling with $f$ -Differential Privacy

The subsampling technique will select a random subset of data to conduct private data analysis. A natural sampling scheme is Poisson sampling, which selects each record with probability  $p$  independently and outputs a subset with random size.

*Definition B.3.* (Poisson subsampling in (Zhu & Wang, 2019)) Given a dataset  $S$  of size  $n$ , the procedure Poisson subsampling outputs a subset of the data  $\{S_i | a_i = 1, i \in [n]\}$  by sampling  $a_i \sim \text{Bernoulli}(p)$  independently for  $i = 1, \dots, n$ .

*Definition B.4.* (Uniform subsampling in (Wang et al., 2019)) Given a dataset  $S$  of size  $n$ , the procedure Uniform subsampling outputs a random sample from the uniform distribution over all subsets of  $X$  of size  $m$ .

Unlike (Lee et al., 2019), which chooses Uniform sampling, we will choose the Poisson sampling scheme in this paper for two reasons. First, compared with Uniform subsampling, Poisson sampling scheme could enjoy a tighter privacy analysis. Theorem 6 in (Zhu & Wang, 2019) shows there is a lower bound for  $\epsilon$  under uniform sampling scheme. While (Wang et al., 2019) proves such lower bound is also an upper bound for Gaussian mechanism when we switch to Poisson sampling. That shows the Poisson sub-sampling scheme is at least as tight as Uniform sub-sampling. Second, Poisson subsampling under GDP has a closed-form expression for privacy budget and noise.

Next, we introduce how to deal with subsampling in  $f$ -DP framework and why the analysis is tight. Realizing that the un-selected data is not released thus in perfect protection, Proposition A.1 in (Bu et al., 2020) states the trade-off function of sub-sampled mechanism satisfies the following property. Let  $f_p := pf + (1-p)Id$  and  $M \circ \text{Sample}_p$  denotes the subsampled mechanism, we have:

$$T(M \circ \text{Sample}_p(S), M \circ \text{Sample}_p(S')) \geq f_p$$

and

$$T(M \circ \text{Sample}_p(S'), M \circ \text{Sample}_p(S)) \geq f_p^{-1}.$$

The two inequalities implies the trade-off function is lower bounded by  $\min\{f_p, f_p^{-1}\}$ . The the trade-off function of  $M \circ \text{Sample}_p(S)$  should be  $\min\{f_p, f_p^{-1}\}^{**}$ , since  $\min\{f_p, f_p^{-1}\}$  is not convex and can not be a trade-off function in general. Where,  $\min\{f_p, f_p^{-1}\}^{**}$  is the double conjugate of  $\min\{f_p, f_p^{-1}\}$ , which is the greatest convex lower bound of  $\min\{f_p, f_p^{-1}\}$  and can not be improved in general. This suggests  $f$ -DP framework could handle subsampling tightly. Moreover, when  $M$  is  $(\epsilon, \delta)$ -DP, (Bu et al., 2020) shows the above privacy bound strictly improves on the subsampling theorem in (Li et al., 2012).

## B.3 Composition with $f$ -Differential Privacy

Another building block for DP analysis of the mixup-based method is composition. When analyzing iterated algorithms, composition laws often become the bottleneck. Fortunately, the  $f$ -DP framework provides the exact privacy bound for the composed mechanism. Specifically, Theorem 4 in (Dong et al., 2021) states that composition is closed under the  $f$ -DP framework and the composition of  $f$ -DP offers the tightest bound. In contrast to  $f$ -DP, (Dong et al., 2021) shows the exact privacy can not be captured by any pair of  $\epsilon, \delta$ . As for moment accountant, which is widely used for analysis of DPSGD, Theorem 1 and Theorem 2 in section 3.2 (Bu et al., 2020) show GDP offers an asymptotically sharper privacy analysis for DPSGD than MA in both  $f$ -DP and  $(\epsilon, \delta)$ -DP framework. (Dong et al., 2021; Bu et al., 2020) also gives a numerical comparison showing the advantage of GDP under the realistic setting of DPSGD.

## B.4 CLT approximation with $\mu$ -GDP

However, calculating the exact  $f$  can be hard especially when  $T$  is large. Fortunately, there exists a central limit theorem phenomenon (Theorem 5 in (Bu et al., 2020)). Intuitively, if there are many ‘‘very private’’ mechanisms, which means the trade-off function are closed to  $Id(\alpha) = 1 - \alpha$ , the accumulative privacy leakage can be described as some  $\mu$ -GDP when  $T$  is sufficiently large. Apart from asymptotic results, Theorem 5 in (Dong et al., 2021) shows a Berry-Esseen type CLT that gives non-asymptotic bounds on the CLT approximation.

## B.5 Connection between $\mu$ -GDP and $(\epsilon, \delta)$ -DP

Dong et al. (2021) shows that  $\mu$ -GDP corresponding to a infinite pairs of  $(\epsilon, \delta)$ -DP. We can use Corollary 1 in Dong et al. (2021) to transform  $\mu$ -GDP to  $(\epsilon, \delta)$ -DP and compare with other DP accountant.

**Corollary B.5.** (Corollary 1 in Dong et al. (2021)) A mechanism is  $\mu$ -GDP if and only if it is  $(\epsilon, \delta(\epsilon))$ -DP for all  $\epsilon \geq 0$ , where

$$\delta(\epsilon) = \Phi\left(-\frac{\epsilon}{\mu} + \frac{\mu}{2}\right) - e^\epsilon \Phi\left(-\frac{\epsilon}{\mu} - \frac{\mu}{2}\right),$$

and  $\Phi(t)$  is the Gaussian cumulative distributive function.

## C Privacy analysis for DPFMix

### C.1 Proof for Theorem 2.1

Here we provide omitted proofs for Theorem 2.1. The following content consists of three parts. First, we need to consider one single step of Algorithm 1. Next, we use the refined composition theorem to bound the trade-off function of the composed mechanism. However, getting the exact solution is computationally expensive. Thanks to the central limits theorem of  $f$ -DP, we can approximate the trade-off function of the composed mechanism with GDP. We will also conduct simulation experiments to show the  $\mu$ -GDP approximation can be quite precise when  $T$  is finite in this section.

#### C.1.1 Single-step of Algorithm 1

**Theorem C.1.** *Let  $\text{Sample}_p(S)$  denotes the Poisson sampling process and  $M$  be the averaging and perturbing process. Then the trade-off function of one step of Algorithm 1  $M \circ \text{Sample}_p$  satisfies:*

$$T(M \circ \text{Sample}_{\frac{m}{n}}(S), M \circ \text{Sample}_{\frac{m}{n}}(S')) \geq \frac{m}{n} G_{\sqrt{1/\sigma_x^2 + 1/\sigma_y^2}} + (1 - \frac{m}{n}) \text{Id}$$

*Proof.* For simplicity, we now focus on a single step and drop the subscript  $t$ . Algorithm 1 release both features and labels and this process can be regarded as first releasing  $\bar{x}$  (denoted as  $M_x$ ) then releasing  $\bar{y}$  (denoted as  $M_y$ ). Therefore we can use the naive composition law of exact GDP (Corollary 2 in (Dong et al., 2021)) to get trade off function  $f$  for generated  $(\bar{x}, \bar{y})$  (denoted as  $M = M_x \circ M_y$ ).

First we consider  $\bar{x}$ , which have  $l_2$ -norm at most  $C_x$  after clipping. Thus removing or adding one record in  $S$  will change  $\|\bar{x}\|_2$  by at most  $\frac{C_x}{m}$ , which means its sensitivity is  $\frac{C_x}{m}$ . So, the Gaussian mechanism  $M$ , which adds Gaussian noise  $\mathcal{N}(0, (\frac{C_x}{m})^2)$  to each elements of  $(\bar{x}_t, \bar{y}_t)$  is  $\frac{1}{\sigma_x}$ -GDP by Theorem 1 of (Dong et al., 2021). The same analysis could be applied to  $M_y$ . Then for  $M$ , we can apply naive composition law for exact GDP (Corollary 2 in (Dong et al., 2021)) and get it is  $\sqrt{1/\sigma_x^2 + 1/\sigma_y^2}$ -GDP. Finally, the trade-off function of  $M \circ \text{Sample}_p$  can be described by Proposition A.1 in Bu et al. (2020).  $\square$

#### C.1.2 Composition

The refine composition law of  $f$ -DP (Theorem 4 in (Bu et al., 2020)) can be used directly for considering the composition in Algorithm 1. Here we could apply it and give proof for Theorem 2.1. Let  $M'$  denotes Algorithm 1.

*Proof.* The size of the DP feature dataset is  $T$ , which means we conduct  $T$  copies of mechanism  $M \circ \text{Sample}_{\frac{m}{n}}$ . Applying the above refined composition theorem, we have:

$$T(M'(S), M'(S')) \geq \left( \frac{m}{n} G_{\sqrt{1/\sigma_x^2 + 1/\sigma_y^2}} + (1 - \frac{m}{n}) \text{Id} \right)^{\otimes T} := f$$

Moreover, if  $S$  can be obtained by removing one record in  $S'$ , we will also have

$$T(M'(S), M'(S')) \geq f^{-1}$$

Combining the two inequalities, the trade-off function is lower bounded by  $\min\{f, f^{-1}\}$ . However, in general,  $\min\{f, f^{-1}\}$  is not convex thus not a trade-off function. We could use the double conjugate  $\min\{f, f^{-1}\}^{**}$  as its trade-off function. Note that  $\min\{f, f^{-1}\}^{**}$  is larger than  $\min\{f, f^{-1}\}$  and can not be improved in general.  $\square$

#### C.1.3 CLT approximation

Although we can have the exact trade-off function  $\min\{f, f^{-1}\}^{**}$ , it is hard to compute. Fortunately, there exists a central limit theorem phenomenon. The composition of many ‘‘very private’’ mechanisms can behave like some  $\mu$ -GDP (see Theorem 5 in (Bu et al., 2020)).

**Theorem C.2.** *(Theorem 5 in Bu et al. (2020)) Suppose sample rate  $p$  depends on  $T$  and  $p\sqrt{T} \rightarrow \nu$ . Then we have the following uniform convergence as  $T \rightarrow \infty$*

$$(pG_{1/\sigma} + (1-p)\text{Id})^{\otimes T} = G_\mu$$

where  $\mu = \nu \cdot \sqrt{e^{1/\sigma^2} - 1}$  (Note that there is a typo in (Bu et al., 2020)).

Here we could use Theorem 5 in (Bu et al., 2020) to prove the second part of Theorem 2.1.

*Proof.* Under the condition of Theorem 2.1, we can apply Theorem 5 in Bu et al. (2020) directly. It gives:

$$\left(\frac{m}{n}G\sqrt{1/\sigma_x^2+1/\sigma_y^2} + \left(1 - \frac{m}{n}\right)Id\right)^{\otimes T} \rightarrow G_\mu$$

, where  $\mu = \nu \cdot \sqrt{e^{1/\sigma_x^2+1/\sigma_y^2} - 1}$ . Since  $G_\mu$  is already a trade-off function,  $\min\{G_\mu, G_\mu^{-1}\}^{**} = G_\mu$  and finish the proof of second part of Theorem 2.1  $\square$

We also compare the asymptotic guarantee with exact numerical results with typical setting of DPFMix and find the approximation is quite accurate even with  $T \approx 200$ . In Figure 5, we numerically calculate the exact  $f$ -DP (red solid) given by Theorem 2.1 and compare with its  $\mu$ -GDP approximation (blue dashed). We follow a typical setting of DPFMix we introduced in Section 4.4. Specifically,  $\mu = 0.5016$  (corresponding to  $(2, 10^{-5})$ -DP) and  $\sigma = 0.8441$ . In the original setting,  $T = n = 50000$  is quite large. To best illustrate the fast convergence, we show the comparison of  $T = n = 10, 50, 200$  respectively in Figure 5. We also adjust  $\frac{m}{n}$  to make all the three cases satisfying 0.5016-GDP. From the left figure, we can see the two curves are getting closer when  $T$  increases. The approximation  $l_2$  and  $l_\infty$  error shown in Figure 6 also have the same trend. That suggests when  $T$  is sufficiently large, the CLT yields a very accurate approximation, which validate the Berry-Esseen type CLT (Theorem 5 in (Dong et al., 2021)). In practice, we often deal with very large  $T$ , for example, 60000 and 50000 for MNIST and CIFAR10 respectively and the CLT approximation should be quite accurate.

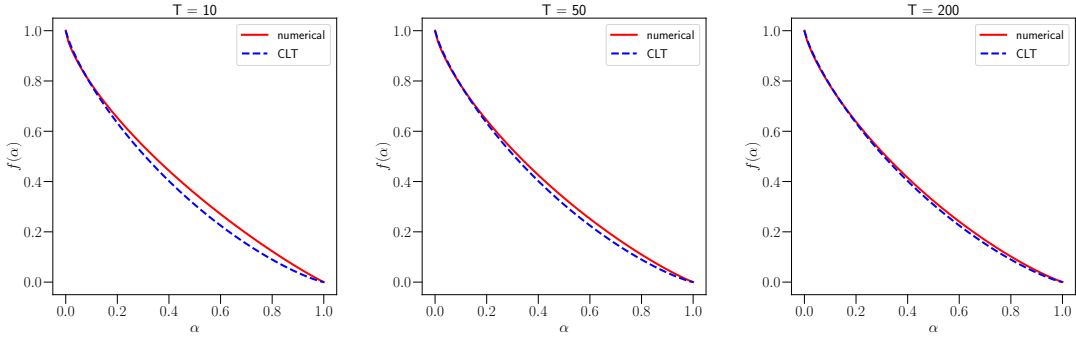


Figure 5: We compare the numerical results of  $\left(\frac{m}{n}G\sqrt{1/\sigma_x^2+1/\sigma_y^2} + \left(1 - \frac{m}{n}\right)Id\right)^{\otimes T}$  with asymptotic GDP approximation. When  $T$  increases, the two curves are getting closer to each other. We also show the approximation error w.r.t.  $T$  in the following Figure 6. That suggests the CLT approximation will be increasingly accurate as  $T$  increase.

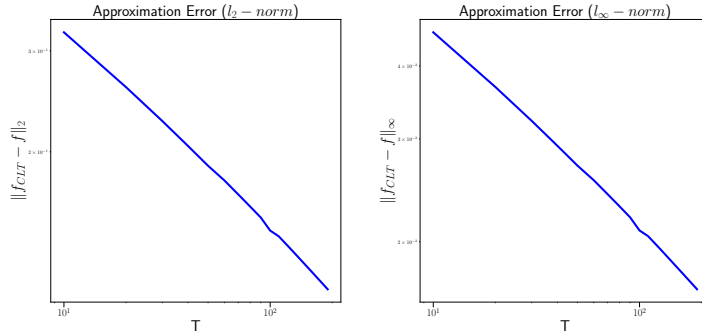


Figure 6: The figures shows the CLT approximation  $l_\infty$  and  $l_2$  error decrease when  $T$  increase.

#### C.1.4 Actual noise

We introduce a hyper-parameter  $\lambda$  and let  $\sigma_y = \lambda\sigma_x$  for balancing DP noise on features and labels. Then the the actual noise  $\frac{C_x}{m}$  and  $\frac{C_y}{m}$  can be written as Lemma C.3 by inverting Theorem 2.1.

**Lemma C.3.** *Let  $\sigma_y = \lambda\sigma_x$ , where  $\lambda > 0$  is a constant. Let*

$$\frac{C_x}{m}\sigma_x = \frac{C_x\sqrt{\lambda^2 + 1}}{\lambda m\sqrt{\ln\left(1 + \frac{\mu^2 m^2}{m^2 T}\right)}}$$

$$\frac{C_y \sigma_y}{m} = \frac{C_y \sqrt{\lambda^2 + 1}}{m \sqrt{\ln \left( 1 + \frac{\mu^2 n^2}{m^2 T} \right)}}.$$

Then, when  $m\sqrt{T}/n \rightarrow \nu$  for a constant  $\nu > 0$  as  $T \rightarrow \infty$ , Algorithm 1 is asymptotically  $\mu$ -GDP.

*Proof.* Note that the  $\ell_2$  sensitivity for features and labels are  $\Delta f_x = \frac{C_x}{m}$  and  $\Delta f_y = \frac{C_y}{m}$  (See proof of Theorem C.1). Then the above expressions are equivalent to  $1/\sigma_x^2 + 1/\sigma_y^2 = \ln \left( 1 + \frac{\mu^2 n^2}{m^2 T} \right)$  and using Theorem 2.1 could get the results.  $\square$

## C.2 DP Guarantee with Renyi-DP

To compare Renyi-DP with the Poisson sampling scheme, we also provide privacy bound for Algorithm 1 here. In experiments, we calculate the RDP privacy budgets using the autodp python package, which is officially released software of Zhu & Wang (2019).

**Theorem C.4.** Given  $n, m, \sigma_x, \sigma_y, C_x, C_y, T$ , Algorithm 1 satisfies  $(\alpha, \epsilon_{RDP}(\alpha))$ -Renyi-DP for integer  $\alpha \geq 2$ , where

$$\epsilon_{RDP}(\alpha) = T \frac{1}{\alpha-1} \log \left\{ \left( 1 - \frac{m}{n} \right)^{\alpha-1} \left( \alpha \frac{m}{n} - \frac{m}{n} + 1 \right) + \sum_{\ell=2}^{\alpha} \binom{\alpha}{\ell} \left( 1 - \frac{m}{n} \right)^{\alpha-\ell} \frac{m^\ell}{n^\ell} e^{(\ell-1) \left( \frac{\alpha}{2\sigma_x^2} + \frac{\alpha}{2\sigma_y^2} \right)} \right\} \quad (4)$$

*Remark C.5.* We can convert RDP to  $(\epsilon, \delta)$ -DP by Proposition 3 in (Mironov, 2017). By minimizing over  $\alpha$ , we can get Algorithm 1 is  $(\epsilon_{RDP}^*, \delta)$ -DP:

$$\epsilon_{RDP}^* = \min_{\alpha \geq 2} \epsilon_{RDP}(\alpha) + \frac{\log(1/\delta)}{1-\alpha}$$

*Proof.* As shown in Appendix H, one step of Algorithm 1 is composed of  $M_x$  and  $M_y$ . For  $M_x$ , it satisfies  $\epsilon_{M_x}(\alpha) = \frac{\alpha}{2\sigma_x^2}$  by Gaussian mechanism in Mironov (2017). For  $M_y$ , it satisfies  $\epsilon_{M_y}(\alpha) = \frac{\alpha}{2\sigma_y^2}$ . Therefore according to Proposition 1 of (Mironov, 2017),  $M$  satisfies:

$$\epsilon_M(\alpha) = \frac{\alpha}{2\sigma_x^2} + \frac{\alpha}{2\sigma_y^2}.$$

Then we consider the composition of subsampled mechanisms. According to Theorem 6 and Proposition 10 in (Zhu & Wang, 2019), Gaussian mechanism applied on a subset from Poisson sampling satisfies  $(\alpha, \epsilon'_{RDP}(\alpha))$ -Renyi-DP for any integer  $\alpha \geq 2$ , where,

$$\epsilon'_{RDP}(\alpha) = \frac{1}{\alpha-1} \log \left\{ \left( 1 - \frac{m}{n} \right)^{\alpha-1} \left( \alpha \frac{m}{n} - \frac{m}{n} + 1 \right) + \sum_{\ell=2}^{\alpha} \binom{\alpha}{\ell} \left( 1 - \frac{m}{n} \right)^{\alpha-\ell} \frac{m^\ell}{n^\ell} e^{(\ell-1)\epsilon_M} \right\} \quad (5)$$

Then the overall privacy leakage can be calculated by the composition law of Renyi-DP (Proposition 1 in (Mironov, 2017)). Therefore, Algorithm 1 satisfies  $(\alpha, T\epsilon'_{RDP}(\alpha))$ -RDP.  $\square$

## D Training with noisy mixup labels

After getting the DP dataset, we can train a differentially private classifier on the DP features. One problem for building a classification model is the noisy mixup label. We solve this problem by first clip the negative values of  $\bar{y}$  to 0 and then minimizing the generalized KL divergence for non-negative vectors  $D(p||q)$ , where  $p$  represents noisy mixup label and  $q$  represents the output of classifier after the Softmax layer.

*Definition D.1.* The generalized KL divergence for non-negative vectors  $p, q$  is defined as:

$$D(p||q) = \sum_i \left( p_i \log \frac{p_i}{q_i} - p_i + q_i \right) \quad (6)$$

with the conventions  $0/0 = 0$ ,  $0 \log 0 = 0$  and  $p_i/0 = \infty$  for  $p_i > 0$ .

## E Implementation Detail of Experiments

### E.1 Datasets

MNIST has 10 categories and each category has 6000 and 1000  $28 \times 28$  grayscale images for training and testing. The colored images of CIFAR10 and CIFAR100 have a spatial size of  $32 \times 32$ . CIFAR10 owns 10 categories and each category has 5000 and 1000 RGB images for training and testing, respectively. CIFAR100 owns 100 categories and each category has 500 and 100 RGB images for training and testing, respectively.

## E.2 Network Structure

In our experiments, we employed the same CNN as Lee et al. (2019). It contains 357,690 parameters and here we list its detailed structure.

Table 5: CNN model used for MNIST, CIFAR10, and CIFAR100, with ReLU activation function.

Layer type	Configuration
Conv2d	32 filters of 5x5, stride 1, padding 2
Max-Pooling	2x2, stride 2
Conv2d	48 filters of 5x5, stride 1, padding 2
Max-Pooling	2x2, stride 2
Fully connected	100 units
Fully connected	100 units
Fully connected	10 units

As for the ScatteringNet Oyallon & Mallat (2015), we follow the setting of (Tramer & Boneh, 2021) for all experiments. We set Scattering Network of depth  $J = 2$ . And use wavelet filters rotated along eight angles. Therefore, for input images with size  $H \times W$ , the feature maps after transformation are  $(81, H/4, W/4)$ . We also conduct group normalization Wu & He (2018) with 27 groups to the features extracted by ScatteringNet.

We also provide detailed configurations of ResNet-50 and ResNet-152 since there are too many variants. ResNet-50 in our paper has 24M parameters and corresponds to the “ResNet-50 1X without Selective Kernel” in (Chen et al., 2020). ResNet-152 has 795M parameters and corresponds to the “ResNet-152 3X with Selective Kernel” in (Chen et al., 2020). The checkpoint of the corresponding model can be download from [gs://simclr-checkpoints/simclrv2/pretrained](https://simclr-checkpoints/simclrv2/pretrained).

## E.3 Detailed Settings for DPFMix and Baselines

**DPMix:** Our implementation of pixel-wise mixup. We tried different networks for DPMix. In Section 4.2, we use the same network described in Lee et al. (2019) to show better privacy accountant could improve the results of Lee et al. (2019). When comparing DPMix and DPFMix, we choose ScatteringNet Tramer & Boneh (2021) described in Appendix E.2 for MNIST to make a fair comparison with DPFMix since we show that ScatteringNet classifier performs better than CNN on MNIST dataset in 7. We choose and the same CNN described in Lee et al. (2019) for CIFAR10/100, because we tried ResNet-50 and ResNet-152 for DPMix on CIFAR10/100 dataset in Table 2 and show larger networks may lead to weaker utility because of overfitting. The experiments in Tables 2 and 6 use modified ResNet-50 and ResNet-152 which have a input size of  $32*32*3$  to keep the dimension for pixel mixup the same as the network described in Lee et al. (2019) to make a fair comparison. While the modification of input size also improves the utility of pre-trained ResNets with  $224*224*3$  input size. For example, the best test CIFAR10 accuracy during training is only 15.64% for pre-trained ResNet-50 with  $(8, 10^{-5})$ -DP. If not specified, we set  $C_x = C_y = 1$ . We train the model with Adam for 200 epochs and batch size 256. The initial learning rate is 0.001 and decays by 10 at epoch 80,120,160. For CIFAR10 and CIFAR100 datasets, we also use standard data augmentation including random horizontal flipping and random crop, on the released images to mitigate overfitting.

**DPFMix:** When we conduct mixup at the feature level, we build a linear classifier upon the mixed features. For MNIST, which contains gray-scale images, we use ScatteringNet Tramer & Boneh (2021) described in Appendix E.2 as the feature extractor and the output size of Scattering Net is  $81*7*7$ . For RGB images, we choose ResNet-50 and ResNet-152 pre-trained on unlabeled ImageNet with SimCLRv2 as feature extractor (Chen et al., 2020). To fit the input size, we resize the images to  $224*224$  and use features with 2048 and 6144 dimensions before the final classification layer. We set  $C_x = C_y = 1$  in all experiments. We train the model with Adam for 200 epochs and batch size 256. The initial learning rate is 0.001 and decays by 10 at epoch 80,120 and, 160.

**Non-private baseline:** Training without considering privacy. The training setting is the same as corresponding methods except for no mixup or noise. It serves as an upper bound of the utility of DP methods.

**DPPro:** This is a DP data publish algorithm that first uses random projection to reduce the dimension then injects noise. To make a fair comparison, we use DPPro algorithm on the same feature as DPFMix and build a logistic regression model on the released dataset. Note that we don’t add noise to label for DPPro. So, DPPro only have DP guarantees on features and release the raw labels. We train the classification model with Adam for 200 epochs and batch size 256. The initial learning rate is 0.001 and decays by 10 at epoch 80,120 and, 160. We also conduct a grid search on the projection dimension from 50, 100, 200, 400, 800, 1600, 3200, 6400, 12800 and report the best test accuracy.

**P3GM:** P3GM (Takagi et al., 2021) is a data publishing algorithm that first trains a VAE with DPSGD, then releases samples generated from the DP VAE. We use the officially released code of P3GM and follow its default setting. The code only offers the hyper-parameter setting for  $(1, 10^{-5})$ -DP, to evaluate P3GM with different privacy

budgets, we only alter noise scale and keep other hyper-parameter fixed. After getting the generated samples, we use the same ScatteringNet classifier as DPFMix for a fair comparison.

## F Omitted experiment results

Table 6: CIFAR10 test accuracy (%) of DPMix and DPFMix with different models. We show the convergence test accuracy before “+” and the improvement of reporting best accuracy during training after “+”.

$\epsilon$	1	2	4	8	NP
DPMix	24.36+5.60	30.37+2.07	31.97+1.72	31.89+3.01	79.22
DPMix ResNet-50	14.48+10.62	18.73+7.98	12.61+8.69	15.52+16.19	94.31
DPMix ResNet-152	20.77+3.99	17.54+11.52	17.06+12.50	15.35+15.31	95.92
DPFMix ResNet-50	75.58+0.36	77.31+0.20	79.02+0.14	80.75+0.04	94.31
DPFMix ResNet-152	87.74+0.29	89.01+0.13	90.21+0.11	90.83+0.04	95.92

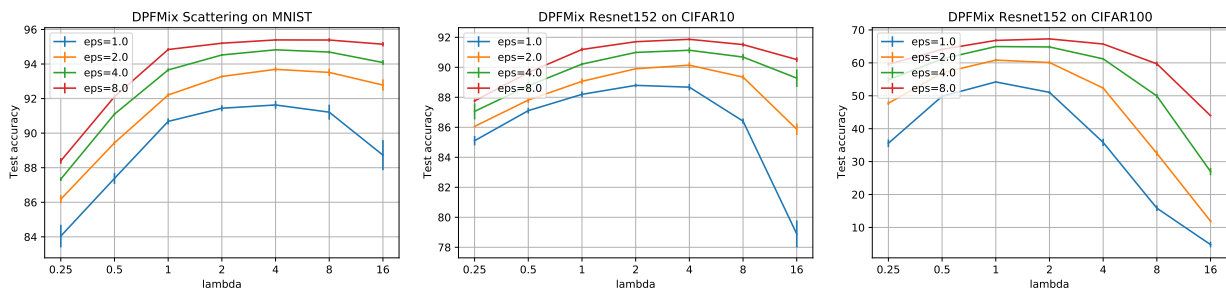


Figure 7: These figures show how utility changed w.r.t.  $\lambda$  under different settings.

Table 7: The table shows MNIST test accuracy (%) of DPMix using CNN or ScatteringNet as classifier, we show the best test accuracy with  $m^*$ . ScatteringNet classifier performs better

	DPMix with CNN	DPMix with ScatteringNet
$\epsilon = 1$	79.19±0.38	82.16±0.54
$\epsilon = 2$	82.71±1.33	83.28±0.53
$\epsilon = 4$	84.09±0.70	84.90±0.26
$\epsilon = 8$	85.71±0.28	86.00±0.28

## G Model Inversion Attack

In this section, we introduce the background of model inversion attack and implementation details. Some visualization results are also shown here. (He et al., 2019) first introduced regularized Maximum Likelihood Estimation (rMLE) to recover the input data in the split learning framework. Under the white-box attack setting, the attackers know intermediate features and the neural network with parameters. Since DPFMix also releases features and does not assume the feature extractor is private, white-box MIA is a proper attack method for DPFMix. We will modify the attack algorithm to adopt mixup setting and show we can defend this type of attack using extensive experiments. Let’s first recall the white-box attack in He et al. (2019). Let  $x_0$  be the original data, original MIA uses an optimization algorithm to find  $\hat{x}$  as the recovered input.

$$\hat{x} = \underset{x}{\operatorname{argmin}} \|f_1(\theta_1, x_0) - f_1(\theta_1, x)\|_2^2 + \lambda TV(x)$$

Where  $f_1(\theta_1, \cdot)$  is the feature extractor,  $TV$  is the total variation loss proposed in (Rudin et al., 1992).

For simplicity, we denote the norm clipping and average process as  $\bar{f}_1$ . For example,  $\bar{f}_1(\theta_1, x_0)$  represent  $\frac{1}{m} \sum_{i=1}^m (f_1(\theta_1, x_0^{(i)}) / \max(1, \|f_1(\theta_1, x_0^{(i)})\|_2 / C))$ . Let  $\bar{TV}(x)$  denotes  $\frac{1}{m} \sum_{i=1}^m TV(x^{(i)})$ . Then, recall that  $\bar{x}_t$  is in the released feature in DPFMix, then the following attack could use the following process to recover the private data.

$$\hat{x} = \underset{x}{\operatorname{argmin}} \|\bar{x}_t - \bar{f}_1(\theta_1, x)\|_2^2 + \lambda T \bar{V}(x)$$

We implement such an attack on MNIST and CIFAR10 datasets with ScatteringNet features since MIA towards a larger model like ResNet-152 could be hard even without feature mixup and DP noise [He et al. \(2019\)](#) (See Appendix Figure 8 for MIA on ResNet-152 features). We use random images sampled from uniform distribution as the initialization of  $x$  and use Adam ([Kingma & Ba, 2015](#)) with  $\lambda = 0.0001$ , the learning rate of 0.1, and maximal steps of 5000 to obtain  $\hat{x}$ .



Figure 8: Attacking from features without mixup and DP noise of ResNet-152 on CIFAR10 dataset. MIA fails to attack such a deep model with 152 layers. This observation meets the one in [He et al. \(2019\)](#)

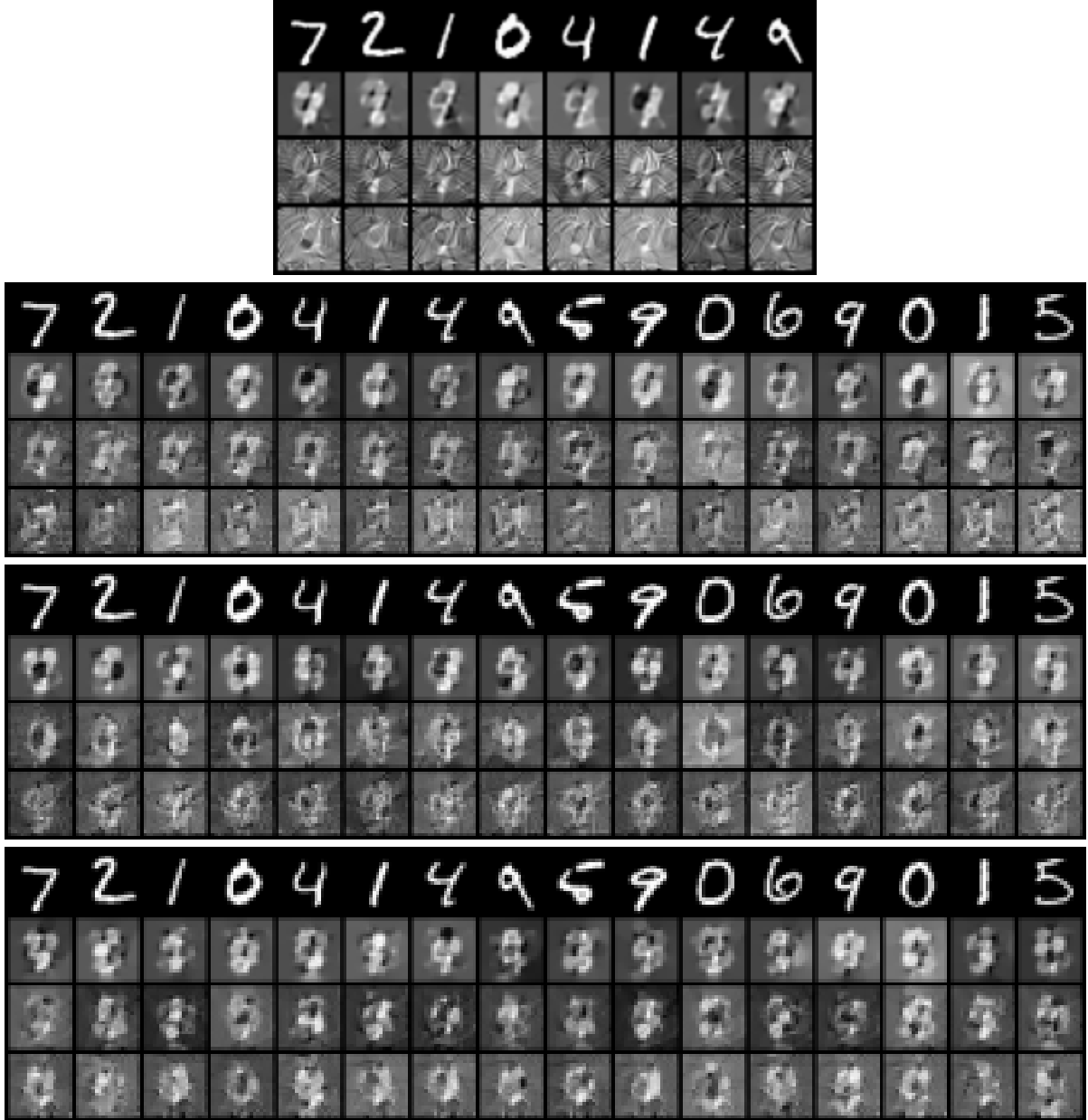


Figure 9: Attacking from features of Scattering net on MNIST dataset. The first row corresponds to raw images, and the following three correspond to recovered images by MIA with  $\sigma = 0$ ,  $\epsilon = 8$ , and  $\epsilon = 1$  respectively. Due to the limited space, we present  $m = 8, 16, 32, 64$  case here and for  $m \geq 16$  cases, we only show the nearest neighbors of the first 16 raw images.

## H Proof of Theorem 3.1

*Proof.* By definition, there holds

$$\begin{aligned}
\tilde{\beta} &= [(MX + E_X)^T(MX + E_X)]^{-1} (MX + E_X)^T(My + E_Y), \\
&= [(MX + E_X)^T(MX + E_X)]^{-1} (MX + E_X)^T[M(X\beta^* + \epsilon) + E_Y], \\
&= [(MX + E_X)^T(MX + E_X)]^{-1} (MX + E_X)^T [(MX + E_X)\beta^* - E_X\beta^* + M\epsilon + E_Y], \\
&= \beta^* + [(MX + E_X)^T(MX + E_X)]^{-1} (MX + E_X)^T(-E_X\beta^* + M\epsilon + E_Y).
\end{aligned}$$

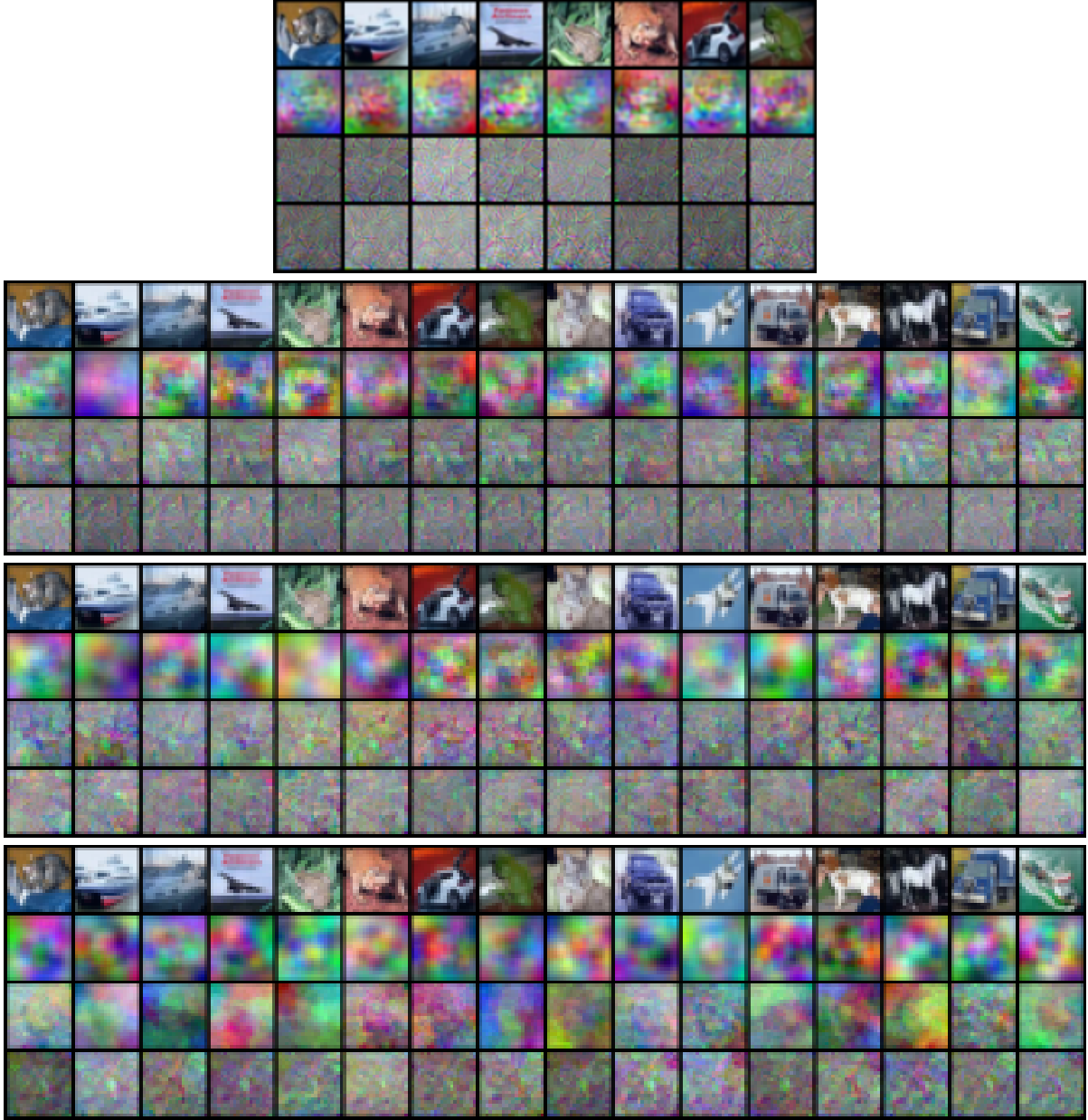


Figure 10: Attacking from features of Scattering net on CIFAR10 dataset. The first row corresponds to raw images, and the following three correspond to recovered images by MIA with  $\sigma = 0$ ,  $\epsilon = 8$ , and  $\epsilon = 1$  respectively. Due to the limited space, we present  $m = 8, 16, 32, 64$  case here and for  $m \geq 16$  cases, we only show the nearest neighbors of the first 16 raw images.

Therefore, there holds

$$\begin{aligned}
\|\tilde{\beta} - \beta^*\|_2 &= \left\| [(MX + E_X)^T(MX + E_X)]^{-1} (MX + E_X)^T(-E_X\beta^* + M\varepsilon + E_Y) \right\|_2, \\
&\leq \left\| [(MX + E_X)^T(MX + E_X)]^{-1} (MX + E_X)^T \right\|_2 \left\| -E_X\beta^* + E_Y \right\|_2 + \dots \\
&\quad \dots + \left\| [(MX + E_X)^T(MX + E_X)]^{-1} (MX + E_X)^T M\varepsilon \right\|_2, \\
&= \sqrt{\left\| [(MX + E_X)^T(MX + E_X)]^{-1} \right\|_2} \left\| -E_X\beta^* + E_Y \right\|_2 + \dots \\
&\quad \dots + \left\| [(MX + E_X)^T(MX + E_X)]^{-1} (MX + E_X)^T M\varepsilon \right\|_2, \tag{7}
\end{aligned}$$

where the last step is by the fact that  $(A^T A)^{-1} A^T [(A^T A)^{-1} A^T]^T = (A^T A)^{-1}$  for all suitable matrix  $A$ .

We first estimate the minimal eigenvalue of  $(MX + E_X)^T(MX + E_X)$ . First of all, for the case that  $n, T \rightarrow \infty$ ,

and  $0 < \lim \frac{n}{T} = \alpha < 1$ , by [Bai & Yin \(1993\)](#) on extreme eigenvalues of random matrices, there holds

$$T \frac{n-m}{mn^2} (1 - \sqrt{\alpha})^2 I_n \preceq M^T M \preceq T \frac{n-m}{mn^2} (1 + \sqrt{\alpha})^2 I_n, \quad (8)$$

with probability going to one when  $n \rightarrow \infty$ .

Secondly, for the case that  $n, T \rightarrow \infty$ , but  $\lim \frac{n}{T} = \alpha = 0$ , we will consider an expansion of  $M$ , marked as  $\tilde{M} \in \mathbb{R}^{T \times (n+\tilde{n})}$ , where  $\tilde{n} \in \mathbb{N}$  satisfy  $\lim \frac{n+\tilde{n}}{T} = 0.01$ . Applying [Bai & Yin \(1993\)](#) again, and there holds for  $\tilde{M}$  that

$$0.81T \frac{n-m}{mn^2} I_n \preceq \tilde{M}^T \tilde{M} \preceq 1.21T \frac{n-m}{mn^2} I_n, \quad (9)$$

with probability one when  $n \rightarrow \infty$ . Note that by definition  $M^T M$  is a main diagonal sub-matrix of  $\tilde{M}^T \tilde{M}$ , thus the maximum and minimum eigenvalue of  $M^T M$  is bounded above and below by respective eigenvalues of  $\tilde{M}^T \tilde{M}$ . Therefore, there further holds

$$0.81T \frac{n-m}{mn^2} I_n \preceq M^T M \preceq 1.21T \frac{n-m}{mn^2} I_n, \quad (10)$$

with probability one when  $n \rightarrow \infty$ , for the case that  $\lim \frac{n}{T} = \alpha = 0$ .

Therefore, combining the two cases above in Eq. (8) and (10), for all  $0 \leq \alpha < 1$ , there holds

$$0.81T \frac{n-m}{mn} (1 - \sqrt{\alpha})^2 \lambda_{\min} I_p \preceq X^T M^T M X \preceq 1.21T \frac{n-m}{mn} (1 + \sqrt{\alpha})^2 \lambda_{\max} I_p,$$

with probability going to one when  $n \rightarrow \infty$ , where as a reminder,  $\lambda_{\min}$  and  $\lambda_{\max}$  are defined respectively to be the lower and upper bound for eigenvalues of  $X^T X$ . Apply a similar matrix expansion argument as shown above on  $E_X \in \mathbb{R}^{T \times p}$ , where  $\frac{p}{T} \rightarrow 0$ , there holds

$$E_X^T E_X \preceq 1.21T \sigma_X^2, \quad (11)$$

with probability one when  $n \rightarrow \infty$ . This further indicates that, with probability going to one when  $n \rightarrow \infty$ , there holds

$$\|E_X^T M X\|_2 \leq \|E_X\|_2 \|M X\|_2 \leq 1.1(1 + \sqrt{\alpha}) T \sqrt{\frac{n-m}{mn}} \sigma_X.$$

Note that for  $\frac{mT}{n^2} \rightarrow 0$ , there holds the following comparison on  $\|E_X^T M X\|_2$  and the minimal eigenvalue of  $X^T M^T M X$ ,

$$\frac{\|E_X^T M X\|_2^2}{\frac{0.81(1-\sqrt{\alpha})^2 T \lambda_{\min}(n-m)}{mn}} \cdot \frac{0.81 \lambda_{\min}(1 - \sqrt{\alpha})^2}{1.21(1 + \sqrt{\alpha})^2} \leq \frac{mn \sigma_X^2}{n-m} = \frac{n C_X^2}{m(n-m) \ln\left(1 + \frac{\mu^2 n^2}{m^2 T}\right)} \leq \frac{n C_X^2}{(n-m)} \frac{mT}{\mu^2 n^2} \rightarrow 0,$$

where the second last step is because  $x \ln\left(1 + \frac{c}{x}\right)$  is an increasing function for  $x > 0$ , and  $\lim_{x \rightarrow \infty} x \ln\left(1 + \frac{c}{x}\right) = c$ . Therefore, with probability going to one when  $n \rightarrow \infty$ , there holds

$$\begin{aligned} (M X + E_X)^T (M X + E_X) &\succeq 0.81 \frac{T \lambda_{\min}(n-m)}{mn} (1 - \sqrt{\alpha})^2 I_p - 2 \|E_X^T M X\|_2 \cdot I_p, \\ &\succeq \frac{T \lambda_{\min}(n-m)}{2mn} (1 - \sqrt{\alpha})^2 I_p. \end{aligned}$$

Therefore, there holds

$$\sqrt{\|[(M X + E_X)^T (M X + E_X)]^{-1}\|_2} \leq \left[ (1 - \sqrt{\alpha}) \sqrt{\frac{T \lambda_{\min}(n-m)}{2mn}} \right]^{-1}, \quad (12)$$

with probability going to one when  $n \rightarrow \infty$ .

What's more, using Eq. (11) and central limit theorem, there holds

$$\| -E_X \beta^* + E_Y \|_2 \leq 1.1 \sqrt{T} \sigma_X \|\beta^*\|_2 + 1.1 \sqrt{T} \sigma_Y,$$

with probability going to one when  $n \rightarrow \infty$ . Therefore, there holds

$$\sqrt{\|[(M X + E_X)^T (M X + E_X)]^{-1}\|_2} \| -E_X \beta^* + E_Y \|_2 \leq \frac{2C_X \|\beta^*\|_2 + 2C_Y}{\sqrt{\lambda_{\min}(1 - \sqrt{\alpha})}} \frac{1}{\sqrt{\frac{m(n-m)}{n} \ln\left(1 + \frac{\mu^2 n^2}{m^2 T}\right)}}. \quad (13)$$

with probability going to one when  $n \rightarrow \infty$ .

Moreover, consider taking expectation on  $\varepsilon$  only, there holds

$$\begin{aligned}
& \mathbb{E}_\varepsilon \left( [(MX + E_X)^T(MX + E_X)]^{-1} (MX + E_X)^T M \varepsilon \right) = 0, \\
& \text{var}_\varepsilon \left( [(MX + E_X)^T(MX + E_X)]^{-1} (MX + E_X)^T M \varepsilon \right) \\
&= \sigma^2 [(MX + E_X)^T(MX + E_X)]^{-1} (MX + E_X)^T M M^T (MX + E_X) [(MX + E_X)^T(MX + E_X)]^{-1}, \\
&\leq 1.21T \frac{n-m}{mn^2} [(MX + E_X)^T(MX + E_X)]^{-1} (MX + E_X)^T I_n (MX + E_X) [(MX + E_X)^T(MX + E_X)]^{-1}, \\
&\leq \frac{4\sigma^2}{n} \frac{(1 + \sqrt{\alpha})^2 \lambda_{\max}}{(1 - \sqrt{\alpha})^2 \lambda_{\min}} I_p,
\end{aligned}$$

with probability going to one when  $n \rightarrow \infty$ .

For simplicity of notations, denote  $\zeta = [(MX + E_X)^T(MX + E_X)]^{-1} (MX + E_X)^T M \varepsilon$ . Note that  $\zeta_i$  is Gaussian random variable for any given  $M$  and  $E_X$ , therefore, with probability going to one when  $n \rightarrow \infty$ , there holds

$$\lim_{n \rightarrow \infty} \mathbb{P}_\varepsilon \left( |\zeta_i| < \frac{2\sigma \ln n (1 + \sqrt{\alpha}) \sqrt{\lambda_{\max}}}{\sqrt{n} (1 - \sqrt{\alpha}) \sqrt{\lambda_{\min}}} \right) = 1.$$

Therefore, there further holds

$$\begin{aligned}
& \mathbb{P}_\varepsilon \left( \left\| [(MX + E_X)^T(MX + E_X)]^{-1} (MX + E_X)^T M \varepsilon \right\|_2 > \frac{2\sigma \sqrt{p} \ln n (1 + \sqrt{\alpha}) \sqrt{\lambda_{\max}}}{\sqrt{n} (1 - \sqrt{\alpha}) \sqrt{\lambda_{\min}}} \right) \\
&\leq \sum_{i=1}^p \mathbb{P}_\varepsilon \left( |\zeta_i| > \frac{2\sigma \ln n (1 + \sqrt{\alpha}) \sqrt{\lambda_{\max}}}{\sqrt{n} (1 - \sqrt{\alpha}) \sqrt{\lambda_{\min}}} \right) \rightarrow 0,
\end{aligned}$$

with probability going to one when  $n \rightarrow \infty$ . Therefore, there holds

$$\left\| [(MX + E_X)^T(MX + E_X)]^{-1} (MX + E_X)^T M \varepsilon \right\|_2 \leq \frac{2\sigma \sqrt{p} \ln n (1 + \sqrt{\alpha}) \sqrt{\lambda_{\max}}}{\sqrt{n} (1 - \sqrt{\alpha}) \sqrt{\lambda_{\min}}}, \quad (14)$$

with probability going to one when  $n \rightarrow \infty$ .

Combining Eq. (7), Eq. (14) and Eq. (13) together, and we will have our final result.  $\square$